A PROCESS FOR REMOVAL OF TOXIC GASEOUS COMBUSTION PRODUCTS FROM SPACECRAFT ATMOSPHERE

BY

GARY PATRICK NOYES

A DISSERTATION PRESENTED TO THE GRADUATE SCHOOL
OF THE UNIVERSITY OF FLORIDA IN
PARTIAL FULFILLMENT OF THE REQUIREMENTS
FOR THE DEGREE OF DOCTOR OF PHILOSOPHY

UNIVERSITY OF FLORIDA

1982

To my parents, who gave me the confidence without which this would not have been accomplished; and to Ellen, my companion on the road through the now into the future, for our children who will play in the worlds we create.

ACKNOWLEDGMENTS

I wish to thank my adviser and committee chairman, John Zoltek, for providing the environment for freedom of scientific enquiry necessary for the conception and execution of this investigation. I also wish to acknowledge the monetary support for this work make possible via a Special Project Grant from the University of Florida Engineering and Industrial Experiment Station.

TABLE OF CONTENTS

PAGE

ACKNOWLEDGMENTS iii

LIST OF TABLES vi

LIST OF FIGURES vii

KEY TO SYMBOLS viii

ABSTRACT xi

CHAPTER

ONE INTRODUCTION 1

- Justification 1
- Toxic Gaseous Combustion Products 6
  - Sources 6
  - Environmental Effects 9
  - Available Techniques for Removal from Gas Streams . . . 12
- Selection of the Process 14
- Plan of the Study 18

TWO CAUSAL ANALYSIS 19

- Driving Forces for Gas-Liquid Absorption Reactions . . . 19
- Kinetics of Mass Transfer at Fluid Surfaces 20
  - Phenomenological Models 20
  - The Lewis-Whitman Model 26
  - A Model for Gas-Liquid Absorption and Reaction 30
- Selection of Gas-Liquid Contact Scheme 31
  - The Staged Countercurrent Column 32
  - The Sparged Bubble Column 33
- The Final Process Model 37
- Solution Compositions and Gas Solubilities 40
- Predictions for Process Behavior 43

PAGE

THREE EXPERIMENTAL METHODS 46

Apparatus and Overall Procedure 46
Procedure for Each Experimental Run 51
Analysis of the Experimental Process 52

Precision and Accuracy 52
Data Reduction 54
Initial Solubilization Transient 56

Experimental Design 57

Gas and Liquid Compositions 57
Statistical Tests and Correlations 60

FOUR DATA AND RESULTS 63

Column Physical Behavior 63
Process Startup Transients 65
Process Steady-State Behavior 67

Sulphur Dioxide 67
Carbon Monoxide 67
Nitrogen Oxides 75

Solubility Dependence of Absorption Rate 78

FIVE CONCLUSIONS AND RECOMMENDATIONS 80

Comparisons of Theory and Results 80
Practicality of the Process 82
The Next Step 84
A New Paradigm 86

REFERENCES 87

APPENDIX A DERIVATION OF DATA REDUCTION EQUATIONS 92

APPENDIX B DERIVATION OF SOLUBILIZATION TIME CONSTANT 98

BIOGRAPHICAL SKETCH 101

LIST OF TABLES

TABLE PAGE

1 Standards for Human Exposure to CO, NO_x, and SO_2 11

2 Solubility of Gases of Interest in Water at 50 C 42

3 Gases and Liquid Compositions for Experimental Runs 59

4 Effects of Liquid Composition on Bubble Column Physical Behavior 64

5 Effects of Liquid Composition on Interfacial Area Parameter 66

6 Time Constants for Column Startup Transients 68

7 Absorption of SO_2 into H_2SO_4-H_2O_2 Solutions 69

8 Absorption of CO into H_2SO_4-H_2O_2 Solutions 70

9 Absorption of CO into HNO_3-H_2O_2 Solutions 71

10 Effects of Gas and Liquid Compositions on F_p for CO Absorption 73

11 Effects of Gas and Liquid Compositions on R_h for CO Absorption 74

12 Absorption of NO_x into HNO_3-H_2O_2 Solutions 76

13 Limiting Absorption Rates for NO_x into HNO_3-H_2O_2 Solutions . 77

14 Correlation of Average R_h with H_p for CO, NO, and SO_2 . . . 79

15 Column Height for 99% Reduction in Pollutant Concentration . 83

LIST OF FIGURES

FIGURE PAGE

1 Pollutant Concentration Profile in Gas-Liquid Absorption and Reaction 20

2 Concentration Profile for Two-Film Model of the Gas-Liquid Interface 27

3 Solubility Equilibrium and Concentration Driving Forces for Two-Film Model of Gas-Liquid Absorption 29

4 Staged Countercurrent Column for Gas-Liquid Contact 34

5 Experimental Apparatus for Investigation of Gas-Liquid Contact 47

6 Independent Variables in the Experimental Design 58

7 Sequential Absorption of SO_2 and NO_x from a Gas Stream . . 85

KEY TO SYMBOLS

a = interfacial area per unit column volume, 1/cm

C_{gp} = pollutant concentration in gas, gmol/l

C_{gpf} = C_{gp} at final or sampling location

C_{gpi} = C_{gp} at column-stage inlet

C_{gpo} = C_{gp} at column-stage outlet

C_{gps} = C_{gp} at standard conditions

C_{la} = acid concentration in liquid, gmol/l

C_{lai} = C_{la} at column-stage inlet

C_{lao} = C_{la} at column-stage outlet

C_{lh} = hydrogen peroxide concentration in liquid, gmol/l

C_{lhi} = C_{lh} at column-stage inlet

C_{lho} = C_{lh} at column-stage outlet

C_{lp} = pollutant concentration in liquid, gmol/l

C^*_{lp} = C_{lp} at gas-liquid interface

d_b = bubble diameter, cm

D_p = diffusivity of pollutant, cm^2/sec

$E°$ = standard electrode potential, volts

f_p = pollutant flux per unit area, gmol/min-cm^2

F_p = pollutant flux per unit volume, gmol/min-cm^3

G = wet gas flowrate, cm^3/min

G_c = gas flowrate through column stage, cm^3/min

G_d = dry gas flowrate, cm^3min

G_{ds} = dry gas flowrate at standards conditions, cm^3/min

G_f = gas flowrate at final or sampling location, cm^3/min

G_i = gas flowrate at column-stage inlet, cm^3/min

G_o = gas flowrate at column-stage outlet, cm^3/min

h_c = column height, cm

H_p = Henry's Law constant or solubility parameter, atm-l/gmol

k = generalized coefficient

k_g = gas-side mass-transfer or film coefficient, $gmol/min\text{-}cm^2\text{-}atm$

k_l = liquid-side mass-transfer or film coefficient, $gmol/min\text{-}cm^2\text{-}atm$

K_g = gas-side overall mass-transfer coefficient, $gmol/min\text{-}cm^2\text{-}atm$

K_l = liquid-side overall mass-transfer coefficient, $gmol/min\text{-}cm^2\text{-}atm$

n = distance in direction of concentration gradient, cm; or sample size

n_d = film thickness parameter, cm

N_p = pollutant molar flowrate, gmol/min

N_{pi} = N_p at column-stage inlet

N_{po} = N_p at column-stage outlet

P = total pressure, atm

P_d = (partial) pressure of dry gas, atm

P_f = total pressure at final or sampling location, atm

P_i = total pressure at column-stage inlet, atm

P_o = total pressure at column-stage outlet, atm

P_p = partial pressure of pollutant in gas, atm

P_p^* = P_p at gas-liquid interface

P_{pi} = P_p at column-stage inlet

P_{po} = P_p at column-stage outlet

P_s = standard pressure (1 atm)

P_v = (partial) pressure of water vapor, atm

P_{vc} = P_v for column-stage liquid

P_{vf} = P_v at final or sampling location

P_{vi} = P_v at column-stage inlet

P_{vo} = P_v at column-stage outlet

P_{vs} = P_v at standard conditions

r = pollutant reaction rate in liquid, gmol/min-cm^3

r^2 = coefficient of determination

R = universal gas constant, 82.1 cm^3-atm/gmol-K

s_1,s_2 = standard deviations of samples

s_p^2 = pooled variance for 2-sample t-test

t = time, sec or min

t = test statistic for small sample analysis

T = temperature, C or K

T_c = column temperature

T_f = temperature at final or sampling location

T_i = temperature at column-stage inlet

T_o = temperature at column-stage outlet

T_s = temperature at standard conditions, 25 C or 298 K

v_g = gas holdup or gas volume per unit column volume

V_c = column-stage volume, cm^3 or liter

V_l = column-stage liquid volume, cm^3 or liter

$\bar{x}_1$, $\bar{x}_2$ = arithmetic means of samples

y = generalized dependent variable (measured value)

$\bar{y}$ = arithmetic mean of y

y' = generalized dependent variable (model value)

α, β, γ = generalized exponents

Abstract of Dissertation Presented to the Graduate
Council of the University of Florida in Partial
Fulfillment of the Requirements for the Degree of
Doctor of Philosophy

A PROCESS FOR THE REMOVAL OF TOXIC GASEOUS COMBUSTION PRODUCTS FROM SPACECRAFT ATMOSPHERE

By

Gary Patrick Noyes

August 1982

Chairman: John Zoltek, Jr., P.E., Ph.D.
Major Department: Environmental Engineering Sciences

The purpose of this study was the selection and evaluation of a process for essentially complete removal from incineration exhaust of the primary toxic gaseous products of organic waste combustion, namely carbon monoxide (CO), sulfur dioxide (SO_2), and nitrogen oxides (NO_x). The process selected for evaluation was staged countercurrent bubble column absorption of these pollutant gases into aqueous hydrogen peroxide (H_2O_2) solutions acidified with the products, mainly sulfuric acid (H_2SO_4) and nitric acid (HNO_3), of pollutant oxidation and hydration in the absorbent solution.

Simulated incineration exhaust containing the pollutant gases was bubbled through a single-stage column of acidified H_2O_2 solutions at constant temperature (50 C) and gas flow. Experiments were performed to determine pollutant outlet concentrations from bubble columns with different pollutant species and inlet concentrations in the gas and

different acid species (H_2SO_4 and HNO_3) and H_2O_2 and acid concentrations in the liquid.

Statistical regressions and tests of hypotheses were used to evaluate process dynamics. Pollutant absorption rate was found to be primarily dependent on pollutant solubility in aqueous solution. Absorption rate was also dependent on gas-phase pollutant concentration and liquid-phase acid type and concentration. Gas-liquid interfacial area per unit bubble column volume was also found to be dependent on acid type and concentration.

Pollutant absorption rate and column interfacial area were very weakly if at all dependent on H_2O_2 concentration. The rate-limiting step for this gas-liquid absorption-reaction process was shown to be pollutant diffusion through the liquid interphase region.

The ratio of calculated fluid heights of bubble columns required to remove equal percentages of NO_x and SO_2 was 400 to 1 respectively. Thus the countercurrent absorption of SO_2 and NO_x from the same polluted gas stream into acidified H_2O_2 solutions could be accomplished sequentially, with intrinsic separation of the product acids H_2SO_4 and HNO_3 as two nearly-pure solutions.

CHAPTER ONE
INTRODUCTION

Justification

The first pictures of the whole Earth seen from deep space were taken by the crew of Apollo 8 in December of 1968. The finite interconnectedness of the Earth's biosphere so evident in these photographs has created a global environmental awareness unparalleled in history. The rapidly growing human population of our planet and consequent competition for a slowly dwindling natural resource base is disquieting, especially in consideration of the continual proliferation of conventional and nuclear weaponary.

Within several generations, we humans probably will have consumed all the readily available energy, industrial, and agricultural resources of "Spaceship Earth." Survival in this scenario will soon require us to stop human population growth and learn to recycle all material wastes into life-support consumables, using only the limited flows of renewable energy available on the Earth.

Another possible future has been created by our expanding knowledge of and ability to function in near-Earth space. Human colonization and industrialization of extra-terrestrial space to exploit the energy and material resources therein for the benefit of the Earth was first proposed and studied by O'Neill [1] in the early 1970's. A substantial body of published studies show that the utilization of near-Earth resources is within the technical capability of several highly industrialized cultures (American, Japanese, Soviet, and Western European) and would yield net material, energetic, and economic resources at a rate sufficient to significantly ease the burgeoning resource crisis of our planet.

Stine [2] performed a detailed survey of possible high-value products which could be manufactured by space industries. He listed 50 processes which are prohibitively expensive or physically impossible in the dense atmosphere and 1-G acceleration field of the Earth's surface, but which may be easily exploited using the hard vacuum (10^{-11} mm Hg or 10^{-13} atm) and microgravity (10^{-3} cm/sec^2 or 10^{-6} G) of near-Earth space. The lack of gravity-driven convective fluid flow in space will allow fundamental study of fluid behavior dominated by only diffusional and surface-active forces, enhancing our understanding of fluid dynamics on Earth [3].

Glaser [4] proposed and studied the large-scale deployment of solar power satellites in geosynchronous orbit (22,300 miles altitude), transmitting photovoltaicly-captured sunlight to Earth as collimated microwaves or laser light. Built in low Earth orbit of terrestrial origin materials, each such satellite in the stationary (with respect to the Earth) orbit would supply, after reception and conversion, 10 GW of electrical power to a fixed point on Earth at competitive busbar rates. The vast potential of this extraterrestrial energy source has generated sufficient interest in government, industry, and academia that a peer-reviewed journal dedicated to the study of this proposal began publication in 1980 [5].

It has been shown [6] that the Moon and near-Earth asteroids have sufficient diversity and abundance of chemical elements to supply the necessary material for fabrication of solar power satellites and for import of substantial quantities of high-value industrial feedstocks (nickel, titanium, rare lanthanide elements, etc.) to the Earth [7]. Transportation systems capable of moving large amounts of material from the Earth, Moon, and near-Earth asteroids to high lunar and terrestrial orbits have been proposed, studied, and their costs estimated [8-10]. Processes for separation of exterrestrial materials into useful elements (metals for structures, silicon for solar cells, oxygen for rocket propellant and life support, etc.) are well within the current state-of-the-art of chemical engineering technology [11]. Fabrication methods for large space structures (solar power satellites and orbital chemical and manufacturing plants) are currently being developed [12].

The economics and time scale for a significant level of space industrialization also appear to be favorable. Indeed, O'Neill [13] showed that the economic "take-off" point (where the rate of return exceeds the rate of investment) for space industrial activity could be reached in 5-7 years with an investment of 25-35 billion dollars, levels of funding and pace comparable to the U. S. Apollo space program.

If implemented, a venture of this magnitude and potential for exponential growth would require many workers to live in space for extended periods of time [14]. The construction of large lunar and orbital habitats for these workers presents no insurmountable structural, mechanical, or thermal difficulties [15, 16]. Since the largest portion of the cost of human activity in space for several decades to come will be transportation [17], space habitats for several hundred or more workers cannot economically run on continual resupply of life-support consumables from the Earth [18]. Human wastes (carbon dioxide, metabolic water, urine, feces, and washwater) generated in such space settlements would have to be transformed into pure oxygen, water, and food for re-use by the crew.

Spurlock and Modell [18] proposed that generalized biotic wastes (human, plant, and animal) could be rapidly and efficiently transformed into inorganic hydroponic nutrient solutions for intensive plant (and therefore animal) production in space habitats, effectively "closing the loop" for life-support consumables. Phillips [19] concluded that a controlled-environment crop and animal production system could be developed for use in space habitats in a decade of sustained effort. This estimate seems reasonable, since most of the produce consumed by the people of harsh, arid Abu Dhabi (on the Persian Gulf) is already being grown via intensive greenhouse hydroponic culture with commercially acquired inorganic nutrient solutions [20]. However, to date no one has demonstrated the feasibility of a process to transform solid and liquid biotic wastes into inorganic salt solutions suitable for hydroponic crop production.

An assessment [21] of candidate designs to fulfill this purpose singled out incineration (flame combustion) as the most rapid and lowest-mass process available for complete oxidation of biotic wastes. This use of incineration would require that the primary toxic gaseous combustion products carbon monoxide, sulfur dioxide, and nitrogen oxides be removed from the carbon-dioxide-rich exhaust before it can be delivered to the hydroponic farm in a large space habitat. Modell [22] proposed the use of an "acid-gas" scrubber which would absorb the exhaust pollutants into a liquid, with subsequent chemical conversion of the pollutants to acids, essentially sulfuric and nitric. These acids could then be reacted with the alkaline incineration ash to produce inorganic salt solutions suitable for hydroponic crop nutrition. Modell said nothing about the nature of the absorbing liquid, or of the process by which the polluted incineration exhaust and the absorbing liquid are brought into contact, or of the manner in which the acids are produced.

The purpose of this study was, therefore, the selection and evaluation of a process for removal of toxic gaseous combustion products from incineration exhaust and conversion of these reduced gases to their oxidized, acidic forms in aqueous solution. For use in spacecraft far from the Earth, such a process must (in descending order of importance):

1. be potentially capable of reducing the concentration of toxic gaseous combusion products below levels harmful to humans, plants, or animals;
2. require no large quantitites of chemical reagents from the Earth; and
3. have rapid throughput, or minimal mass per unit mass of incineration exhaust gas treated per unit time.

Any process with these characteristics would potentially be applicable on the Earth in incineration-based systems for conversion of municipal and agricultural organic wastes into nutrient solutions for hydroponic crop growth. This could help ease the environmental and economic burden of waste treatment and create a renewable supply of fertilizer for the greenhouse crop-production industry.

Selection of a process for the stated purpose must be based on knowledge of the sources, environmental effects, and available techniques for control of toxic gaseous combustion products. Following discussion of these topics, the process chosen for evaluation is described. A brief outline of the investigation concludes this introductory chapter.

Toxic Gaseous Combustion Products

Sources

The toxic gaseous combustion products, hereafter referred to as pollutants, relevant to spacecraft atmosphere as outlined above, arise from three possible sources:

1. incineration of human, plant, and animal waste;
2. production of acids from their gaseous precursours in incineration exhaust; and
3. outgassing from materials used in the interior structure, equipment, and furnishings of the spacecraft.

Since oxygen in a space habitat's atmosphere would be required for incineration, the outgassed pollutants from interior surfaces would become part of the combustion process, possibly increasing the concentrations of pollutants in the incinerator exhaust. However, careful selection of materials for spacecraft interior construction can keep levels of the outgassed pollutants carbon monoxide (CO), sulfur dioxide (SO_2), nitric oxide (NO), and nitrogen dioxide (NO_2) below maximum acceptable concentrations [23].

What is sought is essentially complete conversion of CO, SO_2, and nitrogen oxides ($NO + NO_2 = NO_x$) in incineration exhaust to carbon dioxide (CO_2) and carbonic acid (H_2CO_3), sulfuric acid (H_2SO_4), and nitric acid (HNO_3) in aqueous solution. Mass-balance control in the space habitat would require essentially complete conversion of the carbon, sulfur, and nitrogen in biotic waste to CO_2 and CO, SO_2, and NO_x in the incinerator exhaust. Production of these gases is a function of fuel composition and of combustion conditions in the incinerator, topics reviewed by Niessen [24, pp. 82-102] and Seinheld [25, Chapter 7]. The discussion below is a brief summary of the information contained therein.

The combustion condition most greatly influencing the composition of incineration ash and exhaust is the oxidant/reductant mole or mass ratio, the air-fuel ratio. Variation of this parameter about the stoichiometric air-fuel ratio (SAFR) produces significant changes in the concentrations of residual combustible matter in the ash and exhaust. Below the SAFR (fuel-rich, oxidant-limited mixture), an appreciable quantity of high-carbon char remains in the ash. The exhaust may contain several percent CO, soot, and short-chain hydrocarbon gases. At the SAFR, char in the ash and soot in the exhaust have decreased greatly, but the CO level remains about one percent and nitric oxide concentration has risen somewhat. Just above the SAFR (fuel-lean, excess-oxygen mixture), CO and soot in the exhaust and char in the ash have dropped to low-residual levels, but flame temperature and thermally-driven NO production (from nitrogen in the combustion air feed) have maximized. At air-fuel ratios far above the SAFR, flame temperature is well below maximum and pollutant production has minimized. But under these conditions, combustion is slower, yet more unstable, and requires a prohibitively large volumetric flow of air through an excessively large furnace.

To minimize CO, soot, and char production at as low an air-fuel ratio as possible causes high NO production. Under these conditions, conversion of sulfur and nitrogen in the fuel to SO_2 and NO is essentially complete. Experience with large-scale incineration of generalized organic waste (food garbage, wastepaper, yard trimmings, crop residues, feedlot waste, etc.) indicates that the choice of an operating air-fuel ratio is a trade-off between high levels of CO and high levels of NO. Carbon monoxide concentrations can be reduced to well below one percent (10,000 ppm) by volume with attendent production of several thousand ppm of NO. Nitrogen fixation to NO in the furnace can be decreased to the minimum (from several hundred to several thousand ppm) imposed by oxidation of the nitrogen in the fuel to NO. Essentially all sulfur in the fuel is converted to SO_2, with concentrations in the exhaust from several hundred to several thousand ppm.

Conventional processes for industrial production of sulfuric and nitric acids might be applicable to the reduction of these pollutants in incineration exhaust. This would involve oxidation of the SO_2 and NO to SO_3 and NO_2, followed by water scrubbing countercurrent to the gas flow, thereby hydrating these higher oxides to H_2SO_4 and HNO_3 in aqueous solution. However, concentrations of SO_2 and NO_x in the gaseous effluents of these processes cannot practically be reduced to less than several hundred ppm [26, 27]. Further reduction can only be achieved at the expense of progressively larger and larger oxidation and absorption process units.

Any chlorine and fluorine in incinerator fuel is quantitatively converted to hydrogen chloride and hydrogen fluoride in the exhaust.

These gases are so rapidly converted to hydrochloric and hydrofluoric acids by scrubbing the exhaust with almost any aqueous solution [24, p. 98] that these pollutants present no relevant problem in the context of this study.

Environmental Effects

A conclusion which can be drawn from the discussion above is that the exhaust from complete incineration of generalized organic waste inevitably contains appreciable quantities of the gases CO, SO_2, and NO. The significance of these gaseous pollutants is a result of their interaction with the atmosphere and effect on the physical and biological components of the environment.

Altshuller and Bufalini [28] performed a critical review of the atmospheric chemistry of gaseous and particulate pollutants. The gases CO, SO_2, and NO in polluted atmosphere are slowly oxidized to CO_2, SO_3, and NO_2 via complex reactions with oxygen, ultraviolet light, short-chain olefinic gases, and various aerosols (soot, dust, metallic fumes, etc.). At concentrations less than 1 ppm each of SO_2, NO_x, and reactive olefins, photochemically driven processes in the atmosphere create similar levels of toxic and corrosive oxidants such as ozone and peroxyacetyl nitrate. The higher oxides of nitrogen and sulfur react with water vapor and rain to make nitric and sulfuric acids. Rainfall acts as a vast water scrubber for the atmosphere, cleansing it of gaseous and particulate pollutants. The nitric and sulfuric acids present in rainfall through polluted air significantly lower the pH of the rain, producing the phenomenon known as acid rain.

In a recent review of the causes and consequences of acidic precipitation, Babich et al. [29] cited many effects of acid rain and snow on the environment. In the industrial Northeast and Midwest of the United States, the average pH of precipitation and surface water has decreased from 5.5 to 4.5 over the last 25 years, an order of magnitude increase in the hydrogen ion concentration of the water. In some areas, the pH of surface water has dropped below 4.0, an acidity level at which chronic effects on the environment have become apparent. Decreased algal, zooplanktonic, and soil microbial species diversity, increased leaching of soil nutrients and heavy metals from soil colloids, and accelerated erosion of human artifacts (building facia, monuments, etc.) have become evident. At soil and surface water pH levels below 3.0, acute effects have been observed. Soil microbial activity decreased, and toxic and reproductive effects in fish have been noted. In the most intensely acidic areas, some species of fish have vanished, altering the population density and distribution of their prey and predators.

Health effects on humans are a function of exposure duration and pollutant concentration in the air (see Table 1). If pollutant concentrations exceed acceptable Industrial Limits for over 8 hours, irritation of eyes, throat, nose, and lungs may occur; headache, irritability, and impaired performance have also been reported [30, Chapter 14]. The Space Mean Allowable Concentrations were established by NASA as air quality criteria for healthy adults on space missions up to 3 months in duration [23]. Continuous ambient concentrations of CO, NO_2, and SO_2 in excess of the National Primary Standards have been implicated in mortality from respiratory illness, especially for infants, the aged, and the

TABLE 1. Standards for Human Exposure to CO, NO_x, and SO_2 in the Atmosphere.

Exposure Standard	Exposure Duration	Concentration (ppm by vol.)			
		CO	NO	NO_2	SO_2
Industrial Limit[a]	8 hours	50	25	5	5
Space Mean Allowable Concentration[b]	3 months	20	-	1	1
National Primary Standard[c]	many years	9	-	0.05	0.03

[a] U.S. and WHO values for the workplace [30, Table 14.5].

[b] NASA values for spacecraft [23, Table 2].

[c] U.S. ambient air quality limits [30, Table 15.2].

infirm [31]. Chronic effects at these low pollutant levels have also been observed in plants, resulting in decreased yield for crops [30, Table 13.1].

Thus the existence of sources of CO, NO_x, and SO_2, such as incineration of biotic wastes, in spacecraft intended for missions of great duration, would require that these pollutants be removable from the spacecraft atmosphere to very low levels (below 9 ppm for CO and below 1 ppm for NO_x and SO_2).

Available Techniques for Removal from Gas Streams

Many techniques have been used in industry for removal of CO, NO_x, and SO_2 from gas streams, but seldom have effluent concentrations been achieved that are as low as those required for enclosed environments such as submarines and spacecraft. Since industrial effluent standards are several orders of magnitude higher than the National Primary Standards, no economic justification has existed to attempt essentially complete removal of CO, NO_x, and SO_2 from industrial effluents.

There do exist methods for drastically reducing the concentration of CO in air. Oxidation of residual CO and hydrocarbons to CO_2 and H_2O on solid platinum and palladium catalysts is a standard air-purification technique for submarines and spacecraft [23]. Removal of residual CO from gaseous effluents by absorption into alkaline solutions of palladium-copper oxidation catalysts, with evolution of CO_2, has been successful [32].

Sulfur dioxide in flue gas from fossil-fuel-fired power plants and sulfide-ore roasters has been an industrial problem for many years. Biondo and Marten [33] reviewed many methods for flue gas desulfurization and found that scrubbing with aqueous solutions is the most successful and widely used technique. Hydroxides of ammonia and the alkali and alkaline-earth metals are the absorbents of choice. Although alkaline scrubbing could easily be improved to achieve any desired level of SO_2 reduction, a liquid effluent high in sulfite salts is created by this process. Conversion of the sulfite to sulfate and then to sulfuric acid would require a source of strong oxidant and/or acid, plus a complex reaction and separation scheme to recover sulfuric acid and regenerate the alkaline scrubbing solution. Alkaline scrubbing is therefore not suitable for use in a space habitat, far from sources of industrial chemicals.

It is also possible to adsorb gaseous pollutants onto materials with high surface area per unit volume. Vogel et al. [34] found that alkali and alkaline-earth metal oxides adsorb SO_2 readily, but were quite difficult or impossible to regenerate to their original states. Data presented in several patents [35, 36] indicate that activated carbon can reversely adsorb and desorb sulfur and nitrogen oxides, with capacity decreasing in the order SO_2-NO_2-NO. However, the adsorptive capacity is low enough to require the diversion of excessively massive quantities of carbonaceous material in a space habitat to activated carbon production and use. Reversible NO_x adsorption on commercial zeolite molecular sieves [37] is also quite low. In any case, adsorption-desorption processes act only to concentrate these pollutants from one gas stream to another; conversion to nitric and sulfuric acids is not a capability of such processes.

Kobayashi et al. [38] studied the absorption of low concentrations (250 ppm) of nitrogen oxides by various inorganic and organic reagents in water. They found that the efficiency of NO removal positively correlated with the oxidation ability of the reagent, as measured by its standard electrode potential. Apparently chemical oxidation and hydration of NO to nitrate kept the concentration of the pollutant in the solution below its equilibrium value with respect to the gas stream, thereby promoting further absorption. However, the use of such reagent solutions for incinerator exhaust scrubbing in a space habitat would require separation of the nitrate as nitric acid and regeneration of the scrubbing reagent.

Selection of the Process

In view of the constraints cited above, an ideal process for removal of toxic gaseous combustion products from the exhaust of organic waste incineration in a space habitat would entail absorption of the pollutants into an aqueous reagent solution, within which the pollutants would oxidize and hydrate to their acid forms, with complete disappearance of the reagent. Concentration of the resultant solution by removal of water would yield acids of high strength, suitable for reaction with the incineration ash to produce inorganic salt solutions for crop nutrition. The reagent would have to be easily made from materials available within the closed environment of the space habitat.

It was the basic premise of this study that hydrogen peroxide (H_2O_2) is a suitable reagent for the stated purpose. In aqueous solution, H_2O_2 is a strong oxidizing agent [39], having the electrolytic couple in acidic solution

$$2H_2O = H_2O_2 + 2H^+ + 2e^- \qquad E° = -1.77 \text{ volts} \qquad (1\text{-}1)$$

and in alkaline solution

$$2OH^- = H_2O_2 + 2e^- \qquad E° = -0.88 \text{ volts.} \qquad (1\text{-}2)$$

With their particular gas-liquid contact scheme (few specifications stated), Kobayashi et al. [38] found that reagents with a standard electrode potential E° equal to -0.9 volts effect 10 percent removal of NO from gas streams, while reagents with E° = -1.8 remove about 90 percent of the NO. Since the complete oxidation and hydration of CO, SO_2, and NO_x would yield carbonic, sulfuric, and nitric acids in solution, it is fortuitous that the oxidizing power of H_2O_2 is much higher in acidic solution than in alkaline.

Hydrogen peroxide decomposes to water and oxygen by the reaction

$$2H_2O_2 = 2H_2O + O_2. \qquad (1\text{-}3)$$

Complete consumption of H_2O_2 in solution by reaction with CO, SO_2, and NO_x would produce aqueous solutions of only the acidic forms of these pollutants; no extraneous cations or anions would have to be separated.

Production of H_2O_2 by the commercially-dominant, cyclic alkylanthraquinone process requires as feedstocks only hydrogen and oxygen [40, pp. 487-9]. Both gases could easily be generated in a closed space habitat via electrolysis of water from various sources, such as metabolic and transpired water from organisms, water formed during combustion of waste, etc.

Hydrogen peroxide is completely miscible in water in all proportions, has a low vapor pressure compared to water, and appreciably increases the boiling-point temperature of its aqueous solutions [39, Figure 4], all advantageous properties for contact with heated flue gas. Also, concentrated H_2O_2 solutions carry immense quantities of available oxygen [40, p. 494]; each volume of reagent-grade H_2O_2 (30 percent by weight) contains 110 volumes of oxygen at standard temperature and pressure (STP: 1 atm and 25 C). Assuming complete and equimolar reaction, one cubic meter of 30 percent H_2O_2 (1.11 gm/cm^3 density) could absorb the sulfur dioxide from 220,000 m^3 of gas containing 1000 ppm of SO_2 at STP.

Reactions such as these are the basis of analytical techniques for quantitative determination of SO_2 in stack gases [41, Methods 711 and 712] and the atmosphere [41, Methods 705 and 706] and total NO_x in gas streams [41, Method 407]. Sulfur dioxide is collected by bubble-sparging a measured volume of gas through a known volume of dilute acidified H_2O_2 solution. The SO_2 is oxidized to sulfuric acid, which dissociates to two moles of hydrogen ions and one mole of sulfate ions per mole of SO_2 entering the sparging vessel. The practical lower limits of accuracy (0.05 ppm SO_2 for air and 10 ppm SO_2 for stack gases) are due to interferences by other pollutants. Nitrogen oxides are determined by a batch process, wherein the gas of interest is collected in an evacuated 1000 ml flask containing 25 ml of dilute acidified H_2O_2 solution. One to seven days are required for complete absorption and oxidation to nitric acid. The lower limit of accuracy for this method (50 ppm NO_x as NO_2) is set by the detection threshold of the colorimetric method used to determine the amount of nitrate formed in the absorbing solution.

The pronounced differences in sensitivity (10 ppm for SO_2 versus 50 ppm for NO_x) and gas-liquid contact time (seconds for SO_2 vs many hours for NO_x) indicate that the SO_2-H_2O_2-H_2SO_4 reaction is much more rapid and possibly more complete than the NO_x-H_2O_2-HNO_3 reaction.

The rapid absorption of SO_2 in acidified H_2O_2 solutions has been demonstrated on an industrial scale by Thirion [42]. He passed flue gas upward in countercurrent contact with a liquid stream entering as 15 weight-percent H_2O_2, achieving reduction in SO_2 concentration in the flue gas from 1350 ppm to 10 ppm. The effluent from the bottom of the absorption column contained 20 to 25 percent H_2SO_4 and 0.1 percent H_2O_2.

This process is obviously quite suitable for simultaneous removal of SO_2 from flue gas and production of strong H_2SO_4 solutions. However, Thirion did not provide sufficient data to determine SO_2 absorption kinetics, such as moles absorbed per unit gas-liquid interfacial area per unit time, moles absorbed per unit column volume per unit time, percent reduction in concentration per unit of column height, etc. The dependence of these kinetic parameters on gas-liquid interfacial area per unit volume and on gas and liquid compositions must be determined before the process can be uniquely characterized. The author of this study was unable to locate any published work wherein the rate of absorption of CO and NO_x into acidified H_2O_2 solutions was measured.

Plan of the Study

The goal of this study was the determination of the absolute and relative kinetics of absorption of sulfur dioxide, carbon monoxide, nitric oxide, and nitrogen dioxide from simulated incineration exhaust into aqueous mixtures of hydrogen peroxide, sulfuric acid, and nitric acid. To this end, sufficient theoretical and empirical information was gathered and assessed to generate a hypothetical model of the process, to select the staged countercurrent bubble column as the gas-liquid contact scheme appropriate for the process, and to choose adequate compositional ranges for the gas and liquid mixtures (see Chapter Two below). As described in Chapter Three, an experimental apparatus and procedure were developed to adequately control the independent variables of column pressure and temperature, gas and liquid initial compositions and volumes, etc., and measure the relevant dependent variables of output gas composition, column gas holdup, and bubble size. The behavior of the experimental apparatus was analyzed and data-reduction equations were derived to calculate the kinetic parameters of interest, namely moles of pollutant absorbed per unit column volume per unit time and percent reduction in pollutant concentration per unit column height. Statistical tests and correlations were specified to systematically determine the validity of the hypothetical process model. Data and numerical and logical results of data reduction are presented in Chapter Four. Finally, conclusions reached vis-a-vis the dynamics and practicality of the subject process are stated in Chapter Five, followed by recommendations for future research and an investigative heuristic proposed to speed development of new processes for removal of toxic gaseous substances from gas streams.

CHAPTER TWO
CASUAL ANALYSIS

Driving Forces for Gas-Liquid Absorption Reactions

In the process of gas absorption into a reagent liquid, a gas containing the pollutant is brought into contact with a liquid into which the pollutant will dissolve and chemically react. Reaction reduces the concentration of pollutant in the liquid, allowing more pollutant to dissolve from the gas. The mechanism by which the pollutant in the gas is transformed into its reaction product in the liquid consists of four steps: (1) transport of the pollutant molecules to the surface of the liquid, (2) dissolution into the liquid, (3) transport of the dissolved pollutant molecules into the liquid, and (4) reaction of the dissolved pollutant with the liquid reagent. In order to predict the extent to which the pollutant can be removed from the gas, each of these steps must be characterized.

As shown in Figure 1, the process of gas-liquid absorption and reaction can be conceptually decomposed into several regions, each with distinctly different behavior. The bulk gas phase is considered to be well- mixed and therefore homogeneous, with constant composition at every point in the region at any given instant of time. In the gaseous interphase region, pollutant molecules are transported toward the liquid along a decreasing gradient of concentration. At the gas-liquid interface, pollutant molecules dissolve into the liquid. Movement of the

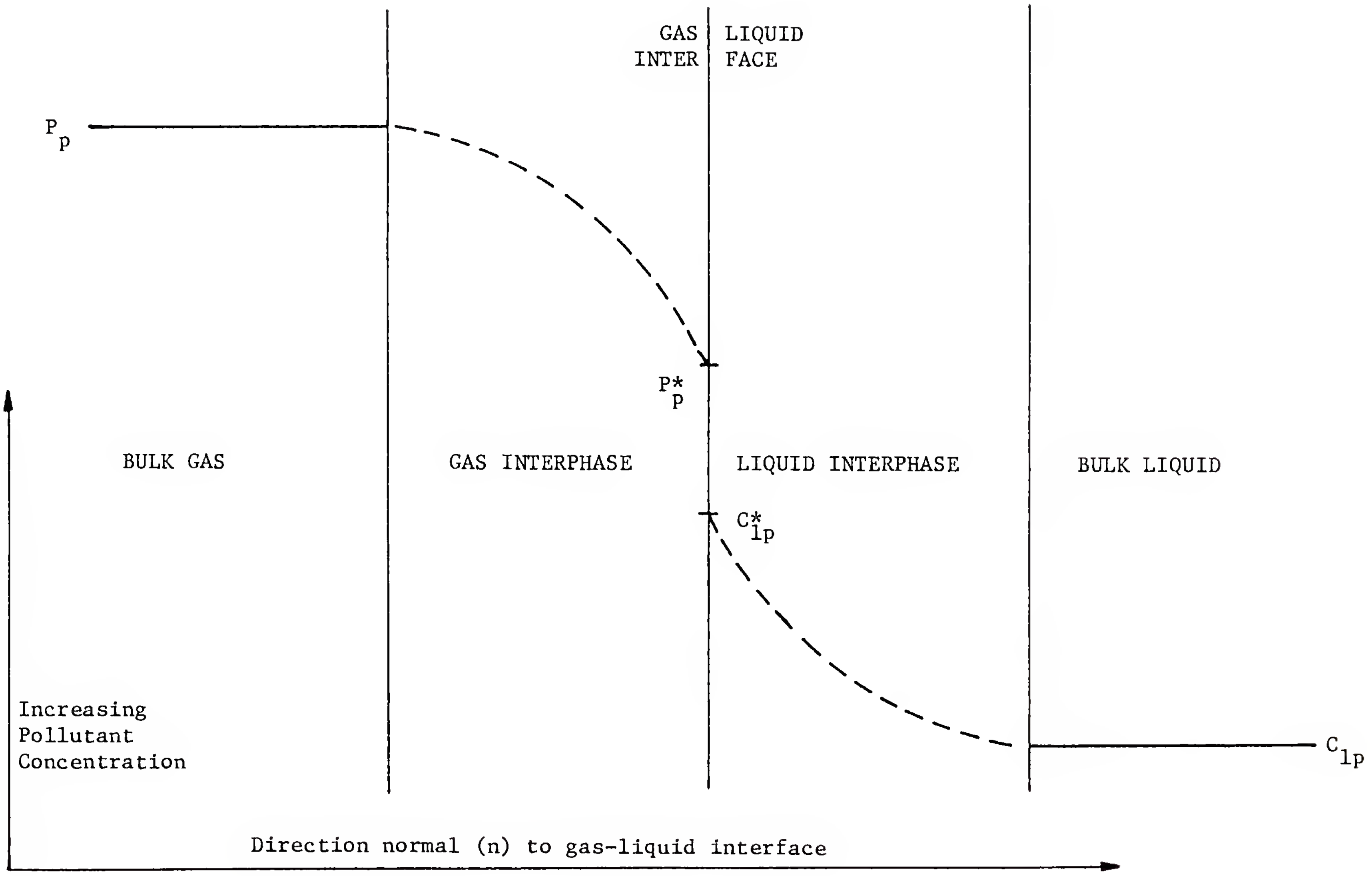

FIGURE 1. Pollutant Concentration Profile in Gas-Liquid Absorption and Reaction.

pollutant through the liquid interphase region is also along a gradient of decreasing concentration. In the bulk liquid, the pollutant interacts homogeneously with the liquid reactant and the reaction products.

For the chemical reaction to proceed in the liquid phase, it must be thermodynamically favorable at the temperature and pressure of the solution. For the particular case studied herein, the reactions of SO_2, CO, and NO with aqueous solutions of H_2O_2 can be separated into several steps, all of which are thermodynamically favorable at near-ambient conditions. The decomposition of H_2O_2 to oxygen and water occurs spontaneously [39], as do the reactions of SO_2, CO, and NO with oxygen to form SO_3, CO_2 and NO_2 [26, 27, 32]. The hydrations of the higher oxides of sulfur and nitrogen to sulfuric and nitric acids in water are also irreversible at near-ambient temperature and pressure [26, 27]. Equilibrium between CO_2 and its hydration product H_2CO_3 is dependent on solution pH; in highly acidic solutions, CO_2 formed via oxidation of CO continually desorbs from the solution [32], thereby limiting the H_2CO_3 concentration to a low level relative to the high concentrations of H_2SO_4 and HNO_3 possible in aqueous solution. Thus from a thermodynamic standpoint, the reactions of SO_2, CO, and NO_x with H_2O_2 in acidified aqueous solution should continually consume these pollutants, allowing more to enter the liquid phase.

The pollutants are all soluble in water to some extent. Solubility equilibrium at the gas-liquid interface is governed by Henry's Law

$$P_p^* = H_p C_{1p}^* . \qquad (2\text{-}1)$$

Henry's constant H_p is truly constant for sparingly soluble gases, such as N_2, O_2, CO, and NO. It decreases with increasing concentration for other gases, such as SO_2, somewhat more soluble in aqueous solution.

In the two interphase regions, the pollutant concentration profile is primarily determined by diffusional transport of the pollutant molecules in response to their concentration gradient. Net diffusional transport is perpendicular to the gas-liquid interface. In accordance with Fick's Law, diffusional flux is proportional to the concentration gradient along this axis, or

$$f_p = -D_p \frac{dC_{1p}}{dn}. \tag{2-2}$$

The minus sign is required to indicate diffusion in the direction of decreasing concentration gradient. The diffusivity D_p for the pollutant in the fluid mixture is for laminar and/or turbulent flow, depending on the dynamic characteristics of the interphase region considered. The diffusivity is also a function of the composition of the gas or liquid in the interphase, and may even vary with changes in the concentration gradient (second-order effect). In any case, the nature of the gas and liquid interphase regions, and the concentration-gradient-driven transport phenomena occurring therein, greatly influence the rate at which gas-liquid absorption takes place.

Kinetics of Mass Transfer at Fluid Surfaces

Conditions in the immediate vicinity of an interface between two fluid phases are difficult to observe or explore experimentally. Two basic approaches to the study of mass transfer at phase boundaries have been used. One approach has been to ignore the nature of the interface regions and to empirically correlate the rate of mass transport through the interface with measurable properties of the bulk phases. The other approach is to develop mathematical models of the process, starting with basic knowledge of microphysical fluid phenomena. The results of the mathematical analyses are then compared with measurable properties in order to assess the validity of the models.

The following discussions of these approaches to understanding mass transfer through phase boundaries have been adapted from reviews by Danckwerts [43, pp. 96-103], Sherwood et al. [44, pp. 150-159], and Treybal [45, pp. 60-66].

Phenomenological Models

The first causal model for mass transfer at fluid surfaces was proposed by Whitman [46] in 1923. He postulated the existence of a stagnant fluid film at the surface of a liquid adjacent to a gas phase. While the bulk of the liquid is kept uniform in composition by agitation, the solute concentration in the film falls from its value C_1^* at the interface to the bulk liquid value C_1 at the inner edge of the film. There is no convection in the film, and the dissolved gas crosses the film by molecular diffusion alone. This simple model predicts for the solute flux

$$f_p = D_p(C_{1p}^* - C_{1p})/n_d. \tag{2-3}$$

The hydrodynamic properties of the system are accounted for by the film thickness parameter n_d, which depends on geometry, agitation intensity, etc.

This model is not very realistic. It assumes the existence of a sharp discontinuity in fluid properties between the film and the bulk liquid, for which no evidence exists. Also, the model suggests no basis for the prediction of n_d, needed to calculate the solute transport rate. However, predictions of mass flux based on the stagnant film model have been remarkably similar to some of those based on more sophisticated models.

The first of these more realistic modes was the "penetration theory" of Higbie [47]. He recognized that, in many situations, the time of exposure of a fluid surface to mass transfer is so short that the concentration gradient of the film theory, characteristic of a steady state, would not have time to develop. He envisioned small fluid elements being brought into contact with the fluid boundary for a fixed time, during which unsteady-state solute transfer occurs at a decreasing rate. The fluid element could be a "particle" of fluid in laminar flow or an "eddy" in turbulent flow. The time of exposure was assumed to be constant for all such eddies or particles of fluid.

The penetration theory predicts that the mass flux should vary as the square root of the diffusivity, whereas the film model predicts linear dependence. The square-root dependence is more realistic in many cases. However, in practice the time of exposure is seldom known, so this model can not predict mass-transfer rates except in special cases.

Danckwerts [48], with his "surface-renewal" theory, extended Higbie's model to encompass a wide spectrum of exposure times for fluid elements at the phase boundary. The gas-liquid interface is then a mosaic of surface elements with different exposure histories. Since the quantity of solute transferred depends on exposure time, the average solute flux for a unit surface area is determined by summation of the values for the individual elements.

Danckwerts assumed that the fractional rate of surface renewal was a constant dependent on hydrodynamic conditions. From this he derived a surface age distribution with which to calculate the solute mass flux. However, since values for the fractional rate of surface renewal are not generally available, the use of this parameter presents the same problems as do the time-of-exposure and film-thickness parameters in the penetration and the stagnant-film theories.

King [49] altered the penetration model to include variable diffusivity, a combination of molecular and eddy diffusivities proportional to some power of the distance from the fluid surface. He retained the concept of a constant time of fluid-element exposure at the interface. This model is even more difficult to use than those already described, since it requires knowledge of two hydrodynamic parameters instead of just one.

Other phenomenological models of mass transfer at fluid surfaces have been proposed. All the existing theories are applicable in some cases, and none are applicable in every case. They are all speculations, and are continually being revised. The ultimate explanation for fluid behavior and mass transfer at phase boundaries awaits elucidation of the fundamental nature of fluid mechanics, one of the few remaining mysteries of physics.

The Lewis-Whitman Model

In light of the lack of generality exhibited by the current theories of interfacial mass transfer, the use of a simple empirical model to characterize a gas-liquid absorption process was justified. The most widely cited model of this type is the two-film concept proposed by Lewis and Whitman [50] in 1924.

The two-film model of the concentration profile for a pollutant being absorbed from a gas into a liquid is shown in Figure 2. Stagnant films are assumed to exist on both sides of the gas-liquid interface. Phase equilibrium for the pollutant species is assumed to exist at the interface, with linear concentration gradients in the two films. Under assumed steady- state conditions, conservation of mass requires that the flux of pollutant molecules from the bulk gas to the interface must equal the flux from the interface to the bulk liquid. Assuming proportionality between flux and concentration gradient in each film,

$$f_p = k_g(P_p - P_p^*) = k_l(C_{lp}^* - C_{lp}), \qquad (2\text{-}4)$$

where k_g and k_l are empirically-determined "film coefficients."

Unfortunately, in mass transfer between turbulent gas and liquid streams, it is virtually impossible to determine the interfacial pollutant concentrations P_p^* and C_{lp}^* . Equation (2-4) is therefore modified to

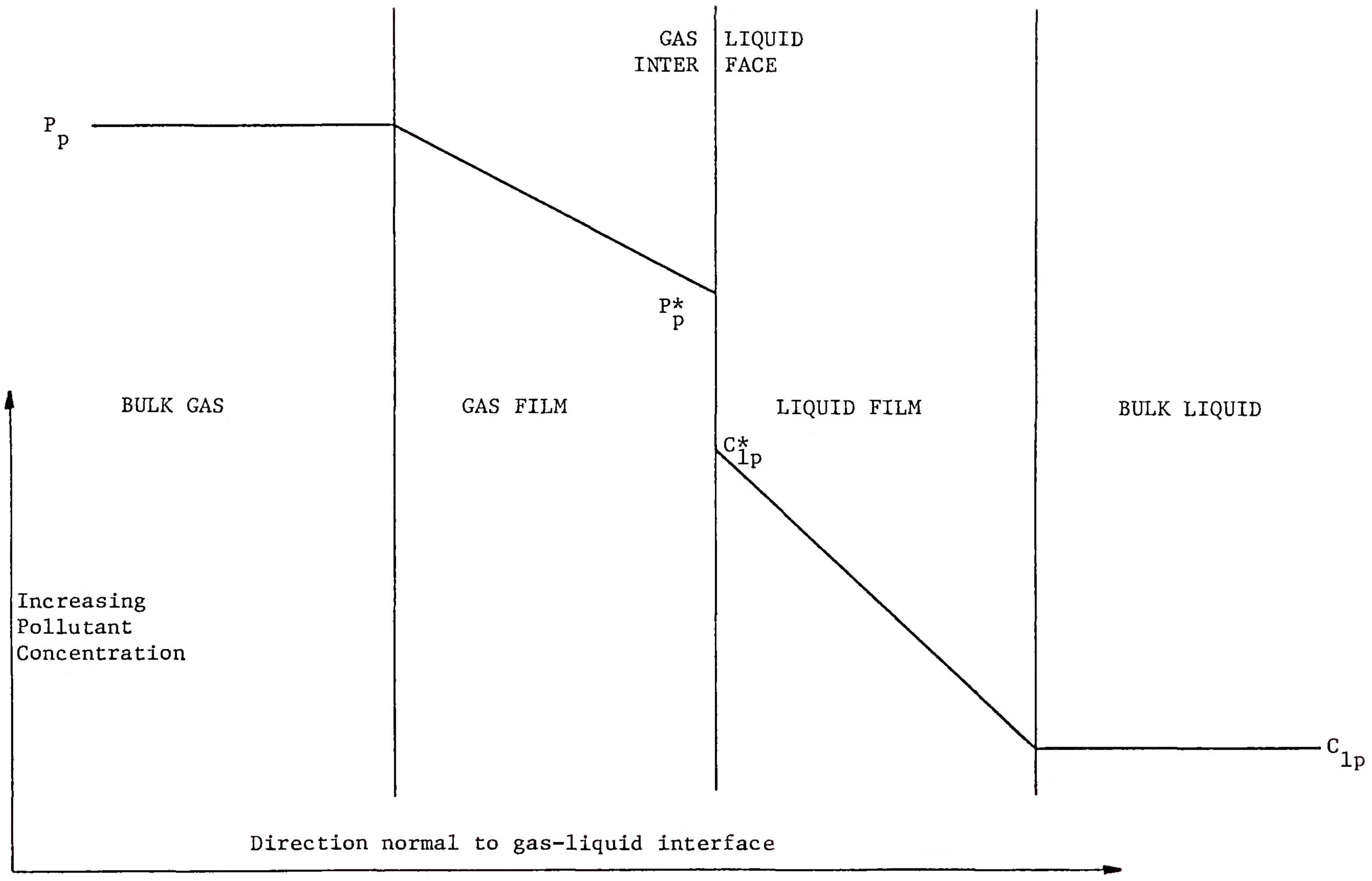

FIGURE 2. Concentration Profile for Two-Film Model of the Gas-Liquid Interface.

$$f_p = K_g(P_p - P_p') = K_l(C_{lp}' - C_{lp}), \tag{2-5}$$

where K_g and K_l are the overall mass-trasnfer coefficients, P_p' is the equilibrium partial pressure of the pollutant over a solution with the bulk pollutant concentration C_{lp}, and C_{lp}' is the concentration in a solution which would be in equilibrium with the bulk gas partial pressure P_p. These relationships are indicated on the solubility-equilibrium diagram of Figure 3.

The point B on the equilibrium curve represents the assumed interfacial composition (P_p^*, C_{lp}^*). The line AB has the slope $-k_l/k_g$ given by

$$k_l/k_g = (P_p - P_p^*)/(C_{lp}^* - C_{lp}). \tag{2-6}$$

When Henry's Law holds, the equilibrium line is straight, and

$$P_p' = H_p C_{lp} \text{ and } C_{lp}' = P_p/H_p. \tag{2-7}$$

The overall coefficients K_g and K_l can be explicitly related to the film coefficients k_g and k_l through (2-4), (2-5) and (2-7) by

$$\frac{1}{K_g} = \frac{1}{k_g} + \frac{H_p}{k_l} \text{ and } \frac{1}{K_l} = \frac{1}{k_l} + \frac{1}{H_p k_g}. \tag{2-8}$$

If the pollutant is very soluble in the solution, H_p is much less than unity; then $K_g = k_g$ and K_l is negligible. In this case, the rate-limiting step in the absorption process is diffusion through the gas film. If the solubility of the pollutant is quite low, H_p is much

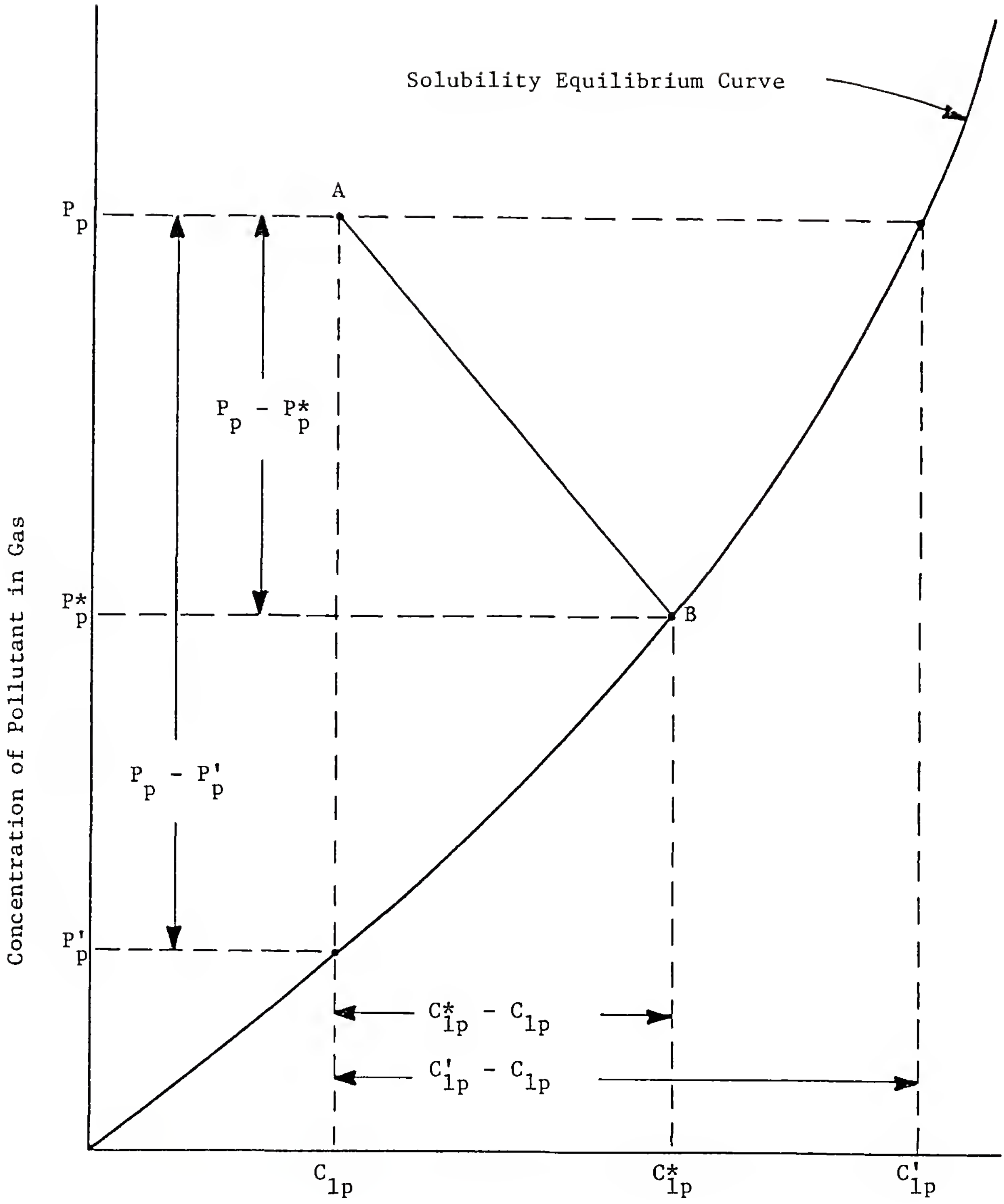

FIGURE 3. Solubility Equilibrium and Concentration Driving Forces for Two-Film Model of Gas-Liquid Absorption.

greater than unity; then K_g is negligible, $K_l = k_l$, and the overall process is controlled by resistance to diffusion in the liquid film. If H_p is close to unity, the rate-controlling film resistance is determined by the relative magnitudes of k_g and k_l.

A Model for Gas-Liquid Absorption and Reaction

The two-film theory described above may more accurately be termed the "two-resistance" theory; a component in the bulk gas must overcome a gas-side resistance and a liquid-side resistance in series to reach the bulk liquid. Scrubbing polluted incineration exhaust with acidified H_2O_2 solutions introduces a third resistance to absorption, in series with the interfacial resistances. If the rate of reaction between H_2O_2 and the pollutants SO_2, CO, and NO_x in solution is slow compared to the rate of absorption, pollutant concentrations in the bulk liquid will increase. This will slow the rate of absorption, establishing pollutant mass-flux balance at a lower level.

The rate of chemical reaction in the bulk liquid is dependent on temperature, pressure, and liquid composition. At constant temperature and pressure, the rate of reaction

$$r = r(C_{lp}, C_{lh}, C_{la}) \tag{2-9}$$

is postulated to be a function of the bulk liquid concentrations of the pollutant, H_2O_2, and possibly the product acid. This rate is expressed as moles of pollutant consumed by reaction per unit volume of fluid per unit time. But the flux of pollutant through the gas-liquid interface is expressed as moles per unit interfacial area per unit time. To find the moles of pollutant passing through the interfacial area in a unit volume per unit time, the flux must be multiplied by the interfacial area per unit fluid volume, or

$$F_p = f_p a. \tag{2-10}$$

Under steady-state conditions, F_p must equal the rate of pollutant consumption per unit volume by chemical reaction, or

$$F_p = r. \tag{2-11}$$

Combining (2-4) and (2-9) through (2-11) gave

$$\begin{aligned} F_p &= k_g a(P_p - P_p^*) = k_1 a(C_{1p}^* - C_{1p}) \\ &= r(C_{1p}, C_{1h}, C_{1a}). \end{aligned} \tag{2-12}$$

This "three-resistance" model was the starting point in this study for characterizing the kinetics of pollutant absorption and reaction with acidified H_2O_2 solutions.

Selection of the Gas-Liquid Contact Scheme

To adequately cleanse polluted incineration exhaust, contact must be maintained between the gas and scrubbing liquid for some period of time to be determined. The manner in which this contact is achieved will greatly affect the phase compositions, the kinetic parameters (interfacial mass-transfer coefficients, interfacial area per unit fluid volume, and the reaction rate), and therefore the pollutant absorption rate.

The Staged Countercurrent Column

There are many ways for gas and liquid to be held in contact for absorption. As in the technique for analytical determination of NO_x in stack gases (cited in Chapter One of this study), both may be held in batch contact until absorption is complete. The gas may be in continuous flow through a batch of liquid, as in the analytical techniques for determination of SO_2 in stack gases and the atmosphere, or both gas and liquid may be in continuous flow. Each phase may be well-mixed and homogeneous, or one or both can be in plug flow. Plug flow of both phases can be co-, cross-, or counter-current to each other.

Due to lack of control over transient startup and shutdown conditions, incineration on an industrial scale is most effectively carried out in a continuous manner. Therefore, a continuous contact process for scrubbing polluted incineration exhaust is required. Continuous gas-liquid absorption in industry is almost invariably carried out in a tower or column with both streams in plug flow [25, p. 425].

Contact between the two phases in a column is usually accomplished in a countercurrent manner. On the average, the differences in the compositions of the gas and liquid phases are greater for countercurrent contact than for either cocurrent or crosscurrent contact. Since the absorption rate is proportional to composition-difference driving forces, countercurrent contact usually requires, for a given rate of gas flow, a shorter column with lower pumping pressures, lower ground loading, etc. A short column would also be most advantageous for use in the restricted geometry of a space habitat, spinning to create centrifugal pseudogravity.

Thus the practical goal of this study was the determination of countercurrent-column height necessary for removal of pollutants from simulated incineration exhaust to a specified level. Since this height was not known beforehand, experimental apparatus to measure it might have encompassed a wide range of column heights. Alternatively, column behavior could be studied in single discrete stages, by varying the gas and liquid compositions into a short column, with a small range of height adjustment. This staged countercurrent absorption column (see Figure 4) was chosen as the best approach to study of the subject process with limited experimental means.

The Sparged Bubble Column

Gas may be brought into intimate contact with liquid in several ways in a countercurrent absorption column. Liquid can flow downward over inert packing, around which the gas rises; sprayed drops can fall in a rising column of gas; or sparged bubbles may rise through a descending column of liquid. The intent in each case is to maximize turbulence and interfacial area per unit volume, to promote the most rapid absorptive flux possible.

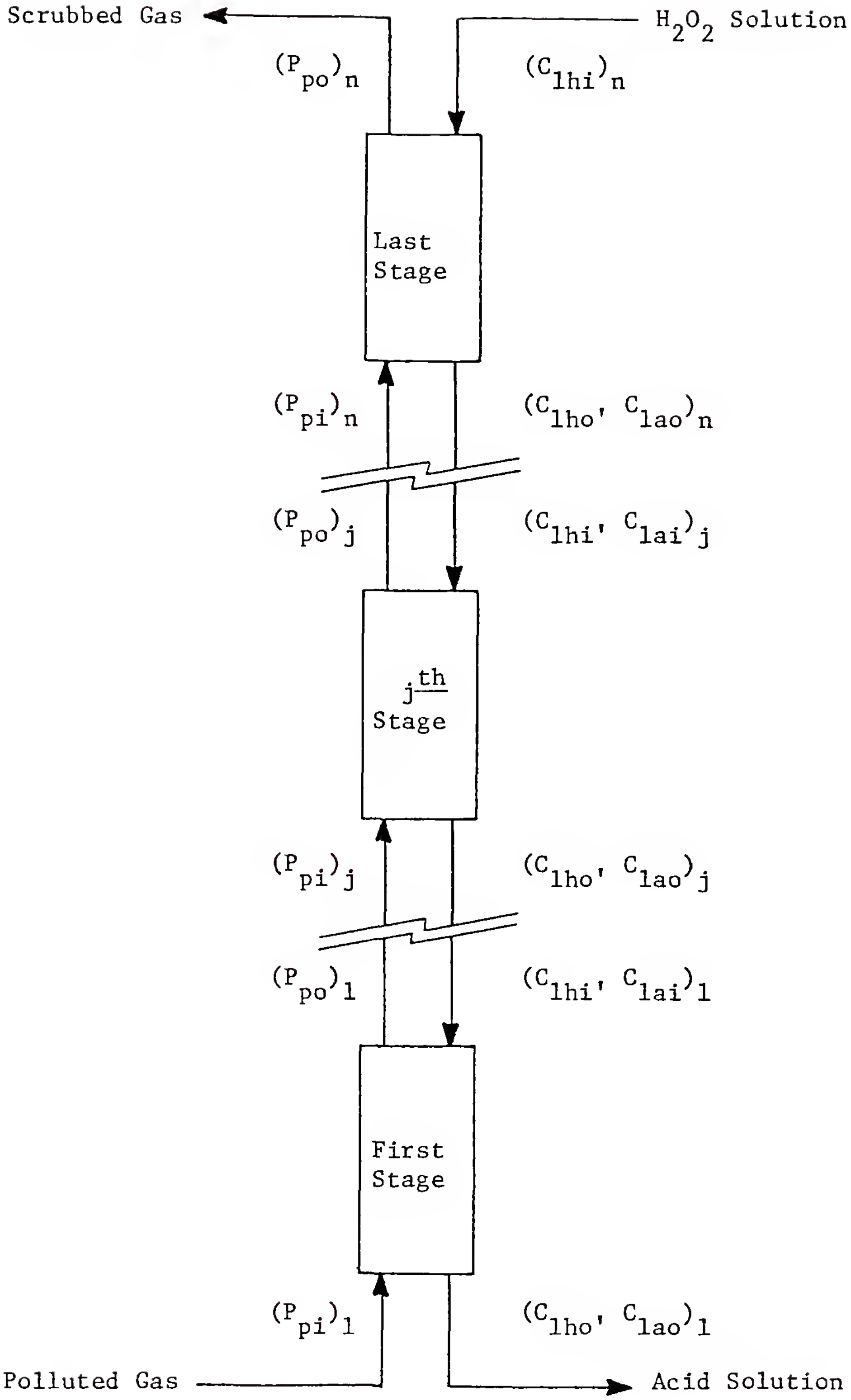

FIGURE 4. Staged Countercurrent Column for Gas-Liquid Contact.

The greatest problem in the applied study of absorption is the difference between the precise laboratory methods of investigation and the practical design of industrial-scale absorption equipment. Experimental apparatus is usually designed for precise control and accurate measurement of microphysical properties, such as interfacial area and local phase compositions, in order to calculate absorptive flux and mass-transfer coefficients. A typical laboratory absorption device is the vertical, transparent wetted-wall tube [51, pp. 691-692], within which the hydrodynamic properties of an annular descending flow of fluid around a rising column of gas can be observed. Staged countercurrent industrial absorbers include the sieve-plate and bubble-cap towers [52, pp. 593-5], in which upward flow of gas through perforated horizontal trays generates bubbles and froth in and on layers of liquid flowing over a vertical sequence of such trays. Flow in these devices is exceedingly complex, and their design is almost an entirely empirical exercise.

For the purposes of this study, a good compromise between the wetted-wall tube and the tray tower was the sparged bubble column. In this device, gas flowing upward through a porous plate (the sparger) disperses as a swarm of small bubbles, rising in a liquid-filled tube. Bubble columns have greater interfacial area per unit volume (more than 5 cm^2/cm^3) than any other gas-liquid contact devices, resulting in compact, low-mass absorption apparatus [44, p. 231]. Data from small-scale bubble-column experiments have been successfully applied to the design of large bubble columns and even sieve-plate towers operated as vertical countercurrent sequences of short bubble columns [43, p. 227].

Basic and applied research on the behavior of bubble columns has been reviewed by Danckwerts [43, pp. 233-235] and Sherwood et al. [44, pp. 651-653]. Agitation in a bubble column is created solely by the rise of bubbles. Liquid back-mixing is rapid, providing uniform liquid composition even for columns with height-to-diameter ratios of 12 or more. For tall, slim columns such as these, bubbles are radially dispersed uniformly and backmixing of bubbles is negligible. This combination of plug flow of the gas phase and complete mixing of the liquid phase is a unique characteristic of bubble columns.

Mass transfer in bubbles is very rapid; the rate of physical absorption without chemical reaction in bubble columns is almost always controlled by the liquid-side resistance. This conclusion is supported by the fact that diffusivities of small molecules are 10^4-10^5 times greater in air than water [53, pp. 13-14]. The liquid-side resistance $1/k_1$ is primarily a positive function of solution viscosity, increasing for viscous liquids such as concentrated sulfuric acid solution.

The interfacial area per unit volume of the bubble column depends on sparger characteristics, gas flowrate, and liquid composition. For a particular sparger and constant gas flowrate, interfacial area per unit volume decreases slightly with increasing liquid viscosity, but increases greatly with increases in solution ionic strength.

This increase in interfacial area is caused by suppression of bubble coalescence. Marrucci and Nicodemo [54] found that the suppression of bubble coalescence in aqueous solutions of inorganic electrolytes was due to the presence of a strong electrical double layer at the gas-liquid interface. They found the repulsion of bubbles to be more closely correlated with the total electrical potential of the interface than with the electrokinetic or zeta potential. Since total and electrokinetic potentials at surfaces are usually not quantitatively related, they concluded that the mechanisms governing bubble coalescence and colloid flocculation must be different.

In any case, the interfacial area for swarms of small bubbles is so vast that Voight and Schugerl [55] found multistage bubble columns to be particularly useful for gas absorption with coalescence-suppressing liquids. Since H_2O_2 solutions, acidified with the strongly dissociating electrolytes HNO_3 and H_2SO_4, should suppress bubble coalescence, the countercurrent multistage bubble column was particularly suitable for the purposes of this study.

The Final Process Model

The three-resistance model (Eqn. 2-12 above) is the most general mathematical description of gas-liquid absorption with chemical reaction. If one of the three series resistances is much greater than the other two, it becomes the rate-limiting resistance for the entire series.

As indicated in the previous section of this chapter, diffusion through the gas interphase region is almost never the rate-limiting step in gas absorption with bubble columns. Also, reactions of hydrated forms of common inorganic gases in electrolyte solutions are sufficiently rapid that interfacial resistance almost invariably limits the rate of absorption of these gases into such solutions [43, p. 260]. In particular, the oxidations of sulfite [56] and nitrite [57] to sulfate and nitrate in H_2O_2 solutions are quite rapid and complete. For the batch determination of NO_x in flue gases, pollutant absorption rate was found not to be limited by reactions in dilute acidified H_2O_2 solutions [58].

Due to the above evidence, it was hypothesized that diffusion through the liquid interphase region should control the absorptive flux of SO_2, CO, and NO_x into acidified H_2O_2 solution in bubble columns. This premise reduced the three-resistance model (2-12) to

$$F_p = k_1 a(C_{1p}^* - C_{1p}). \tag{2-13}$$

Since rapid reaction in the bulk liquid should reduce its pollutant concentration C_{1p} to a very small value relative to the liquid-side interfacial concentration C_{1p}^*, (2-13) became

$$F_p = K_1 a C_{1p}^*. \tag{2-14}$$

From (2-1), solubility equilibrium at the gas-liquid interface

$$C_{1p}^* = P_p^*/H_p \tag{2-15}$$

implied that (2-14) should be

$$F_p = k_1 a P_p^*/H_p. \tag{2-16}$$

But the small gas-side resistance $1/k_1$ causes the pollutant partial pressure P_p^* at the interface to be only negligibly less than the bulk-gas value P_p. Therefore, (2-16) became

$$F_p = k_1 a P_p / H_p. \tag{2-17}$$

For the experiment design of this investigation (see Chapter Three), total pressure P in the bubble column was maintained at near-ambient values. In this case, the gas-phase ideality assumption

$$P_p = y_p P \tag{2-18}$$

was applicable, and (2-17) became

$$F_p = (k_1 P) a y_p / H_p. \tag{2-19}$$

With P (and H_p) expressed with units of standard atmospheres, the numerical value of P approximated unity, and the hypothetical process model became

$$F_p = k_1 a y_p / H_p. \tag{2-20}$$

This model is supported by some experimental evidence. Mehta and Calvert [59] found, for constant interfacial area and gas concentration, that the absorptive fluxes of CO_2 and other low-molecular-weight gases into aqueous suspensions of activated carbon were directly proportional to the solubilities of the gases in water. Voight and Schugerl [55] determined the absorptive flux of oxygen into various dilute aqueous solutions in bubble columns to be positively correlated with both gas-phase oxygen concentrations and interfacial area per unit volume.

For acidified H_2O_2 solutions, the interfacial area parameter of the process model is most dependent on solution composition, particularly the concentration of strong-acid electrolytes [54]. Since H_2O_2 is only weakly acidic [60, p. 293], its contribution to the total ion concentration in highly acidic solutions is negligible. Therefore, the interfacial area per unit volume should depend more on the concentration C_{1a} of strong acids than the concentration C_{1h} of H_2O_2 for highly acidic solutions in bubble columns.

Solution Compositions and Gas Solubilities

The overall reactions of the pollutants SO_2, CO, and NO_x with H_2O_2 are

$$SO_2 + H_2O_2 = H_2SO_4 \tag{2-21}$$

$$CO + H_2O_2 = H_2CO_3 \tag{2-22}$$

$$NO + \frac{3}{2}H_2O_2 = HNO_3 + H_2O \tag{2-23}$$

$$NO_2 + \frac{1}{2}H_2O_2 = HNO_3. \tag{2-24}$$

These reactions would, on the average, consume one mole of H_2O_2 for each mole of pollutant consumed or acid produced. The use of concentrated H_2O_2 solutions to scrub polluted incineration exhaust should yield equally concentrated solutions of acids. Since equilibrium with CO_2 in the exhaust would severely limit the H_2CO_3 concentration in the scrubbing solution, the acid content of this liquid would be primarily H_2SO_4 and HNO_3.

At midheight in a countercurrent absorption column, the scrubbing solution would have high concentrations of both H_2O_2 and the acids H_2SO_4 and/or HNO_3. This situation is unacceptable; high concentrations of H_2O_2 and HNO_3 together make an explosive mixture which rapidly evolves NO_2 [61], while mixtures of concentrated H_2SO_4 and H_2O_2 together evolve considerable amount of H_2O_2 [42]. To avoid these effects, concentrations of H_2O_2 and these acids must be limited to 15-20 percent by weight or about 3-6 gmol/l, depending on the constituent.

These concentrations are still high enough to possibly create multicomponent effects, which might alter the solubility parameter H_p for each gas from its pure-water value. Available correlations for H_p in multicomponent solutions [62, pp. 355-9] are based on values of H_p for binary mixtures of all components in the gas-liquid system. Since solubility data for all possible binary mixtures of the components in the subject process were unavailable, such correlations could not be used.

This difficulty was ameliorated somewhat by the fact that H_2O_2 and its aqueous solutions possess, in general, the same solute and solvent relationships that water alone possesses [60, p. 293]. Therefore, as a first approximation, values of H_p for pure water were used in this study.

These values for gases of interest in this study are shown in Table 2; 50 C is the column temperature at which the experiments of this investigation were performed (see Chapter Three). Since the solubilities of SO_2, CO, and NO vary so widely, the pure-water assumption for H_p

TABLE 2. Solubility of Gases of Interest in Water at 50 C.

GAS[a]	P_p (atm x10^6)	C_{1p} (gmol/l x10^6)	H_p[b] (atm-1/gmol)
N_2	780,000	384	2,030
CO	10,000	7.3	1,370
O_2	10,000	9.4	1,060
NO	10,000	14.3	700
CO_2	200,000	3,930	50.9
SO_2	15,800	15,600	1.01
"	6,180	7,820	0.790
"	1,710	3,110	0.550
"	1,000	-	0.504
"	100	-	0.442
"	10	-	0.436

[a] Data (P_p and C_{1p}) for N_2, O_2 and CO_2 adapted from [63, Table 7-4]; data for CO and NO adapted from [64, Table 3-121]; data for first three lines for SO_2 adapted from [64, Table 3-145].

[b] Values of H_p for N_2, CO_2, O_2, CO, NO, and first three lines for SO_2 calculated using $H_p = 4.35 \times 10^{-1} + 7.10 \times 10^{-5} P_p - 2.19 \times 10^{-9} P_p^2$ (second-order fit to first three SO_2 points).

should not greatly effect the proposed proportionality between absorption rates and solubilities for these gases.

The solubility parameter for NO_2 is not shown in Table 2. This value is very difficult to measure, since NO_2 in contact with water reacts with it to form HNO_3 and NO [44, p. 347]. However, it may be estimated by comparison of the effects [65] of NO and NO_2 on the response of the conductometric apparatus for SO_2 determination (see description in Chapter One of this study). One ppm of NO (H_p = 700 atm-l/gmol) caused a response equivalent to 0.024 ppm SO_2, while one ppm of NO_2 was equivalent to 0.036 ppm SO_2. Greater response meant greater solubility, or smaller H_p. Assuming linearity in this comparison gave H_p = 470 atm-l/gmol for NO_2 and an average H_p = 585 atm-l/gmol for NO_x, as first approximations.

Predictions for Process Behavior

The process model (Eqn. 2-17) indicates that the pollutant absorptive flux is proportional to both the liquid-side mass-transfer coefficient and the interfacial area per unit volume. In general, values for these parameters cannot be predicted by the use of deterministic formulae [43, p. 235]. Many correlations using dimensionless measures of process dynamics have been attempted, but all lack generality [66]. The process model can only be used to make semi-quantitative predictions for the behavior of the process.

The interfacial area per unit volume of a bubble column stage should be roughly proportional to the acid concentration C_{1a} of the aqueous scrubbing solution. Since the absorptive flux F_p should be directly proportional to the interfacial area parameter, F_p should also positively correlate with C_{1a}. Increases in the pollutant partial pressure and its solubility in water should also increase the absorptive flux. The solubility parameter H_p should have the greatest influence on F_p, and the H_2O_2 concentration C_{1h} should have the least effect.

These predictions should hold for SO_2 and CO. However, the process model is not very descriptive of NO_x absorption into H_2O_2 solutions acidified with HNO_3. Having reviewed the voluminous available literature on reactions of NO_x with aqueous HNO_3 solutions, Sherwood et al. [44, pp. 346-361] concluded that the oxides of nitrogen from N_2O to N_2O_2, and also HNO_2 and HNO_3, all play important roles in reaction and diffusion processes in both the gas and liquid interphase regions. The presence of H_2O_2 would further complicate the situation. Since the process model used in this study is based on the assumption of no chemical reactions in the gas phase, this model is inapplicable to NO_x absorption into H_2O_2-HNO_3 aqueous solutions.

An entirely empirical method was used to characterize NO_x absorption in a staged bubble column. The absorption rate was determined as the percent removal R_h per unit of column height. This parameter has more practical significance than the absorptive flux F_p per unit of column volume. A multiple regression technique was used to quantify the dependence of R_h on gas and liquid compositions.

Statistical tests were performed to assess the validity of the hypothesis that interfacial area per unit volume of bubble column is more strongly influenced by solution acid content (type and concentration) than by oxidant H_2O_2 content. The hypothetical process model was evaluated for CO absorption via statistical tests of the relationships among F_p, pollutant partial pressure in the gas, and liquid composition. Similar statistical tests of the relationships between R_h and the independent variables y_p, C_{la}, and C_{lh} for CO absorption were performed to elucidate the dependence of model validity decisions on the use of inlet/outlet concentration ratio R_h versus difference F_p. The predicted primary dependence of absorption rates on gas solubility was evaluated by use of a regression between H_p and R_h for all the pollutant gases studied.

CHAPTER THREE
EXPERIMENTAL METHODS

Apparatus and Overall Procedure

The experimental apparatus (see Figure 5) used in this investigation was designed to generate simulated incineration exhaust, bubble it through a tubular column charged with absorbent solution, and condition the scrubbed gas stream for pollutant concentration determination. The apparatus internal volume, from regulators to final shutoff valves, was capable of being evacuated to 5 mm Hg (0.007 atm) and pressurized to 2 atm (1 atm gauge pressure) without significant leakage.

The simulated incineration exhaust composition was chosen to reflect stoichiometric combustion conditions. The gas composition used was 78 percent nitrogen and 22 percent carbon dioxide, with no oxygen. Actual incineration exhaust contains considerable water vapor. However, whether simulated or actual, water vapor in incineration exhaust equilibrates with the mostly aqueous absorbent solution immediately upon entering a bubble-column gas scrubber. Therefore, the use of dry gas does not unduly compromise the realism of the experiments described herein.

Each source of compressed gas was acquired in steel cylinders from Union Carbide Corporation's Linde Division. Each had less than 10 ppm of extraneous constituents. The cylinders of SO_2, CO, NO, and NO_2 in N_2 were custom-mixed for this investigation. Composition was nominally

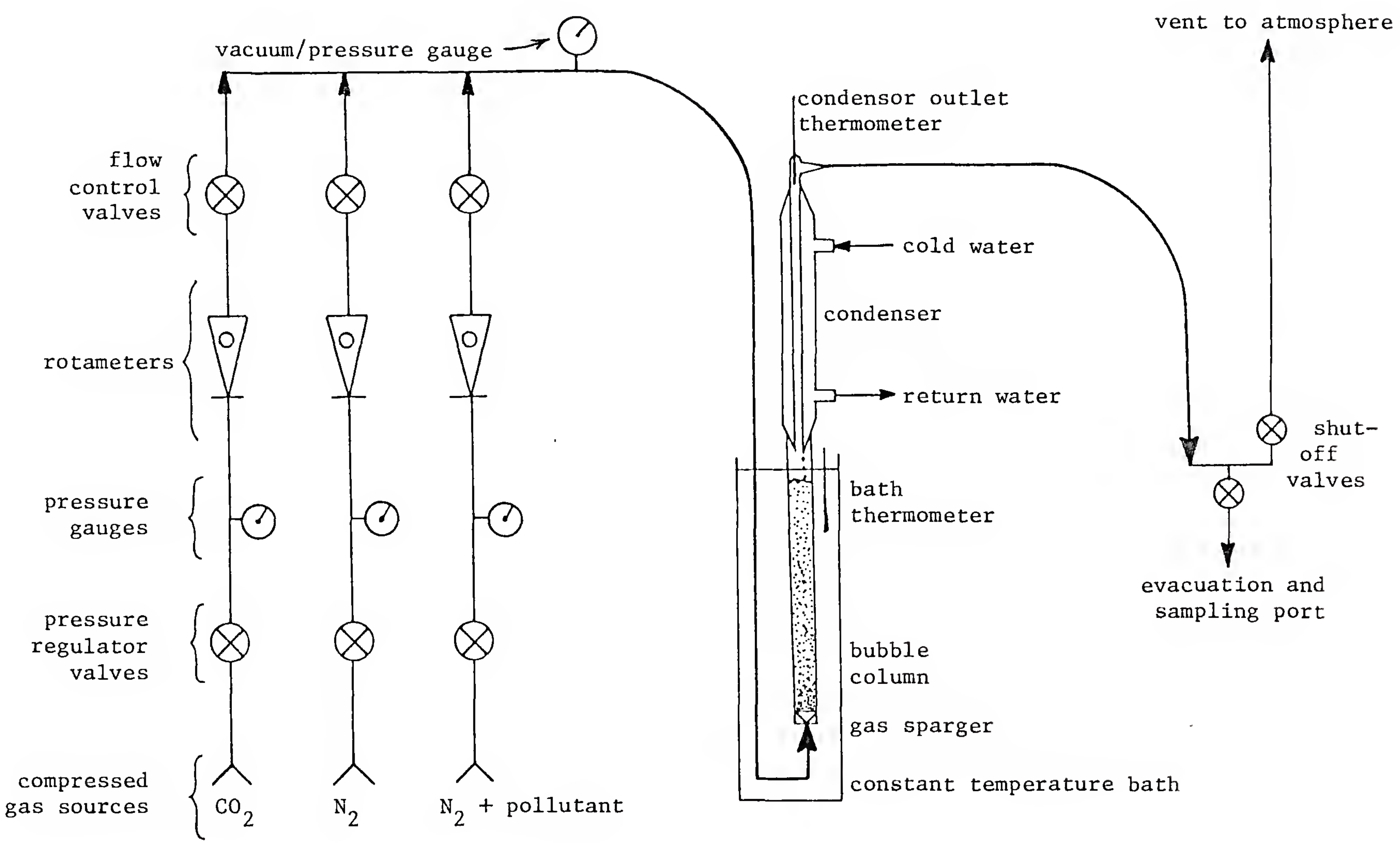

FIGURE 5. Experimental Apparatus for Investigation of Gas-Liquid Absorption Kinetics.

1300 ppm of each pollutant in pure N_2; a certified analysis by the vendor was acquired for each pollutant source. By varying the N_2 and polluted N_2 flow rates, the concentration of pollutant was variable from 10 to 1,000 ppm without variation in N_2 or CO_2 concentration.

The gas-pressure regulator valves were used to maintain 15 psi within the rotameters. Each rotameter measured gas flowrate via dynamic positioning of a glass bead in a graduated vertical glass tube, with internal cross-sectional area increasing from bottom to top. Gas flow through each rotameter was controlled by a precision needle valve downstream of the rotameter. Gases were mixed in a manifold downstream of the needle valves. A combination vacuum/pressure gauge was located between the manifold and the absorption column to insure adequate evacuation and leakage integrity and to measure the column upstream pressure during an experimental run.

All gauges, valves, rotameters, tubing, and fittings in contact with polluted exhaust were made of 316 stainless steel, borosilicate glass, Teflon, or fluoro-elastomer (seals and valve packing). All rotameters were calibrated with a mercury-seal piston flowmeter by the manufacturer, Matheson Corporation. All pressure gauges were calibrated by the author with a mercury manometer.

The absorption column was constructed of identical sections of borosilicate glass tubing, each 15 cm long with 24/40 standard taper joints, lightly coated before fitting with fluorocarbon grease. Column height was varied by adding or removing one or more of these sections. Gas was dispersed as bubbles in the liquid by a porous glass sparger disc (25-50 um pore size, 1 cm in diameter) at the column inlet. Column internal diameter was about 2.5 cm, and column height was variable from 1 cm to 75 cm to keep the pollutant output concentration within detection limits.

The absorption column was immersed in a glass-walled water bath, maintainable at a constant temperature by a thermostatic device. Both the column and the bath were made of clear glass in order to observe bubble flow pattern and diameters via photography. Bubble diameter measurements were calibrated using a photograph of a short ruler inside the water-filled column; this minimized optical distortion introduced by the curved glass walls of the column and water bath.

The bubble column temperature was maintained at 50 C for all absorption experiments. A single temperature was chosen for all experiments, since an increase in the number of independent variables from 3 to 4 would have increased the number of experimental runs from about 50 to over 100. The selected temperature, midway between the freezing and boiling points of water, was a compromise between chemical kinetic limitations at low temperatures and thermodynamic limitations at high temperatures.

Gas leaving the liquid at the column outlet rose through a condenser, kept cool by a flow of cold tap water in its jacket countercurrent to the gas flow. The gas always exited the condenser at ± 2 C of room temperature, the length of tubing from the condenser outlet to the sampling port being sufficient to allow equilibration of gas temperature to ambient, as measured by a thermometer adjacent to the sampling port.

Equilibration of the gas flow to room temperature and $\leq$100% relative humidity was necessary due to temperature constraints on the accuracy of the analytical method for pollutant concentration determination. The measurement technique employed gas-solid reactions with packed granular reagent in small glass tubes. The length of reagent color change, caused by drawing a known volume (50 or 100 cm^3) of polluted gas through the tube with a small piston pump, was calibrated at room temperature (20 C) with known pollutant primary standard gas mixtures by the manufacturer, Bendix-Gastec Corporation.

The reaction employed for carbon monoxide determination was oxidation of CO to CO_2 by palladium palladosulfite, the reduced palladium effecting a color change from yellow to dark brown. Sulfur dioxide was absorbed by a moist sodium hydroxide reagent, the resulting reduction in pH causing the indicator phenol red to change from pink to yellow.

Nitrogen oxides were analyzed with two tubes connected in series. Reaction of NO_2 with white o-tolidine to yield yellow nitros-o-tolidine occurred in the first tube. In the second, NO was oxidized to NO_2 by chromic acid, with the NO_2/o-tolidine reaction indicating the precursor NO concentration.

The known concentrations in the compressed pollutant gas sources were used to re-calibrate the detector tubes to allow for any peculiar ambient or procedural conditions of the experimental mileau. The N_2 and CO_2 gas sources were each tested with the detector tubes at the sampling port for presence of any of the subject pollutants, with negative results. It was found that evacuation of the experimental apparatus to about 5 mm Hg absolute pressure for 5 minutes would remove all measurable traces of pollutant, while at the same time thoroughly drying the interior surfaces.

The reagents 30-percent H_2O_2, 96-percent H_2SO_4, and 69-percent HNO_3 used to mix the absorbent solutions were analytical grade; triply distilled water was the major constituent of the acidified H_2O_2 solutions used in this investigation.

Procedure for Each Experimental Run

Each experimental determination of pollutant removal was run with a single value each for gas-phase pollutant concentration and liquid concentrations of H_2O_2 and acid. The technique for apparatus manipulation and the timing of events during each run were carefully executed so as to be as identical as possible for all runs.

Preparation for each run began by bringing the water bath up to operating temperature. All needle valves were opened fully for 2 min to fill the lines from the source cylinders to the manifold with the source gases. Then the apparatus from needle valves to vent was flushed with N_2-CO_2 gas mixture at maximum available flowrate for 5 min, followed by evacuation to 5 mm Hg for 5 min. The N_2-CO_2 flow was re-established at the common experimental rate of 150 cm^3/min. The condenser was then removed, exposing the column outlet for addition of liquid.

The absorbent solution was mixed, 200 cm^3 poured into a graduated cylinder, and the cylinder placed in a small water bath held at 70 C. When the solution temperature reached 50 C, its volume was measured and recorded, and the proper amount was quickly pipetted into the bubble column. The condenser was replaced and polluted gas flow initiated at the proper flowrate and concentration.

Three detector tubes were used to sample the scrubbed and cooled gas stream at 10, 15, and 20 minutes after initiation of pollutant gas flow. During this time period, condenser outlet and room temperatures and bubble column height were measured and recorded, the bubble pattern was photographed, and water bath temperature and gas flowrates were monitored. Each detector tube reading was recorded immediately after the gas sample was pulled through the tube. After the third sample was taken, the apparatus was flushed with N_2-CO_2 mixture for 5 min. Then the condenser was removed, the solution discarded, the column rinsed, and the condenser reinstalled. Evacuation of the apparatus for 5 min completed the experimental run.

Analysis of the Experimental Process

Precision and Accuracy

The most precisely controlled and accurately measured characteristic of the experimental process was the bubble column water bath temperature; variation was ± 0.1 C. Condenser outlet temperature varied by ± 2 C, and room temperature was in the range of 24 ± 3 C. Pollutant concentrations in the source gas mixtures were certified by the vendor to be accurate to ± 2 percent of the analyzed value, nominally 1300 ppm. All experiments were run within 3 months after the pollutant sources were analyzed. Data presented by Wechter [67] indicated that SO_2, CO, NO, and NO_2, in pure N_2 in steel cylinders, are stable for this duration if the pollutant concentrations are greater than 1000 ppm.

Samuelson and Harman [68] found that contact of polluted combustion exhaust with stainless steel and borosilicate glass negligibly alters the pollutant concentration in the gas. The use of Teflon tubing for gas transport in analytical monitors for the subject pollutants attests to its suitability for this purpose.

Pressure gauges were calibrated to ± 1 percent of full scale values (1 atm gauge). Rotameters were certified by the manufacturer to be accurate to ± 1 percent of full-scale flow rates, resulting in estimated pollutant concentration deviations of ± 5 percent from calculated values. Plug flow in the meter-long segment of 1/4" O.D. tubing, from manifold to bubble column inlet, insured adequate mixing of the source gases.

Total gas flow rate into the bubble column was held at a constant value of 150 cm^3/min, a rate low enough to produce stable bubble-flow pattern with consistent bubble size for all runs with each different absorbant solution. Bubble size measurements were difficult; bubble diameter d_b was estimated to have a possible error range of ± 25 percent.

Column height measurements were accurate to ± 1 mm, resulting in about ± 15 percent error in column gas holdup v_g (gas fraction of column volume). Interfacial area per unit volume

$$a = 6v_g/d_b \qquad (3\text{-}1)$$

was therefore only about ± 40 percent accurate, the least certain quantity used in the investigation. Precision for these parameters was much better, an estimated ± 20 percent for all runs with identical absorbent solutions.

All glassware in contact with H_2O_2 solutions was conditioned by sequential overnight soaking in 15 percent HNO_3 and 30 percent H_2O_2 solutions. This treatment minimized catalytic decomposition of H_2O_2 on the borosilicate glass surfaces [60, p. 171]. Also, the decomposition rate for H_2O_2 in highly acidic, but otherwise pure, aqueous solutions has been found to be less than 0.1 percent per hour for H_2O_2 concentrations from 1 percent to 10 percent [60, pp. 525-528]. Accuracy of liquid concentrations of H_2O_2 and acid was determined by the volume change due to mixing and heating to be about ± 2 percent maximum.

As received from the vendor, the pollutant detector tubes were found to be in error by as much as ± 50 percent. However, precision of tube readings was much better; the three tube readings for each run never varied by more than ± 10 percent of the average reading for the three. Since the detector tubes were recalibrated using the pollutant gas sources of known concentration as standards, their accuracy was probably comparable to their precision. The average corrected reading for the three tubes used in each experimental run was therefore taken as the final or sampling-port pollutant mole fraction y_{pf} (ppm X 10^{-6}) for the run.

Data Reduction

The molar rate of pollutant removal F_p per unit volume in a bubble column is related to column volume and input and output pollutant concentrations and gas flow rates by

$$F_p = (C_{gpi}G_i - C_{gpo}G_o)/V_c. \tag{3-2}$$

As derived in Appendix A, this measure of pollutant removal rate was related to final concentration y_{pf} and final water vapor pressure P_{vf} by

$$F_p = \{y_{ps} - [y_{pf}/(1 - P_{vf})^2]\} G_{ds}/RT_sV_c. \tag{A-15}$$

From the known P_v vs T relationship for water and the final temperature t_f, P_{vf} was easily calculated. The dry gas flow rate G_{ds} was that produced at the apparatus manifold, expressed at standard conditions of temperature (25 C) and pressure (1 atm).

The percent removal R_h of pollutant per unit column height is a more practical measure of process performance than F_p. To compare percent removal rates for all runs, R_h was defined in terms of pollutant concentrations y_p at the column inlet and outlet expressed at standard conditions, or

$$R_h = [(y_{pis} - y_{pos})/y_{pis}] \ 100/h_c. \tag{3-3}$$

As shown in Appendix A, this became

$$R_h = \{1 - [y_{pf}/y_{ps}(1 - P_{vf})^2]\} \ 100/h_c. \tag{A-26}$$

Since R_h is a ratio rather than a difference of concentrations, it should be less dependent on detector tube calibration errors than F_p.

Calibration of the detector tubes was accomplished by passing polluted gas of known concentration through pure water in the bubble column. After equilibration, the final concentration y_{pf} was related (see Appendix A) to the known concentration y_{ps} by

$$y_{pf} = y_{ps}(1 - P_{vf})^2. \tag{A-29}$$

This relationship was employed with data from the calibration runs to generate correction plots for detector tube readings.

Initial Solubilization Transient

When pollutant first contacts fresh liquid in an absorption column, its concentration in the liquid is zero. As more and more pollutant dissolves into the liquid, its concentration in the liquid and the outlet gas rises until the steady-state value, characteristic of the particular experimental conditions, has been reached. Samples taken before this initial transient behavior has passed will not reflect steady-state performance of the process.

With the assumption that the bubble column initially acts as a single equilibrium stage, the output pollutant concentration over time was derived in Appendix B to be

$$y_{po} = y_{pi}\,[1 - \exp\,(-t/t_c)], \tag{B-9}$$

where t_c is the time constant for this transient response curve. After a time equal to $5t_c$,

$$y_{po} = 0.993\ y_{pi} \cong y_{pi}, \tag{B-14}$$

and steady-state conditions have been reached.

The assumption of negligible vapor pressure for the liquid in the column produces conservatively large estimates for t_c. In this case,

$$(t_c)\max = V_1 RT_s / G_{ds} H_p . \qquad \text{(B-13)}$$

This relationship was used to estimate the time $5t_c$ necessary for the steady-state regime of process behavior to be reached. Note that t_c does not depend on pollutant inlet concentration y_{pi}.

Experimental Design

Gas and Liquid Composition

The independent variables used in this study to characterize process dynamics were pollutant type (SO_2, CO, NO, and NO_2), acid type (H_2SO_4 and HNO_3), pollutant concentration y_{ps}, H_2O_2 concentration C_{1h}, and acid concentration C_{1a}. A minimal set of choices for the 3 quantitative variables is the array shown in Figure 6.

This design allowed the maximum amount of information to be generated from a minimum number of experimental runs for each pollutant. Hypotheses about the dependence of F_p (and R_h) on y_{ps}, C_{1a}, and C_{1h} could be evaluated with a small-sample statistical test (see next section of this chapter). Also, the addition of a single run at the center of the cubic array for each of the pollutants NO and NO_2 provided sufficient information to generate a minimal correlation of NO_x percent removal R_h with the 3 quantitative independent variables.

The gas and liquid compositions experimentally employed are shown in Table 3. The order-of-magnitude difference between the low and high

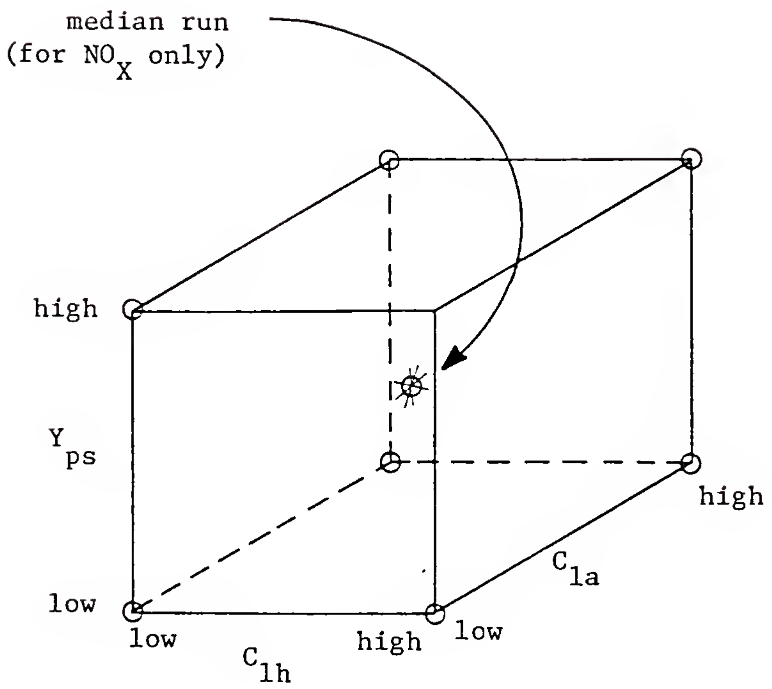

FIGURE 6. Independent Variables in the Experimental Design.

TABLE 3. Gas and Liquid Compositions for Experimental Runs.

	y_{ps} (ppm)			C_{1h} (gmol/1)			C_{1a} (gmol/1)		
GAS	low	median	high	low	median	high	low	median	high
SO_2	100	-	1000	0.5	-	5.0	0.4	-	4.0
CO	200	-	2000	0.5	-	5.0	0.4	-	4.0
NO_x	100	316	1000	0.5	1.58	5.0	0.4	1.26	4.0

values for y_{ps}, C_{1a}, and C_{1h} should reveal the dependence of absorption rate F_p or R_h on these variables, if such dependence exists. Pollutant concentrations for CO were chosen to be greater than for SO_2 or NO_2 because of less stringent standards for removal of CO from gaseous effluents (see Table 1).

Values of concentration variables for NO_x median runs were chosen to be the geometric means of the extreme values. As described below, the appropriate correlation for NO_x absorption then became one which could be easily linearized.

Statistical Tests and Correlations

The small-sample t-test for equality of population means was chosen as the statistical technique applicable to evaluation of F_p and R_h dependence on y_{ps}, acid type, C_{1a}, and C_{1h}. For each of these independent variables, division of the cubic array in Figure 6 by a plane perpendicular to that variable's axis yielded two samples with 8 data points each. The test statistic then became, for a 95 percent confidence interval,

$$t = (\bar{x}_1 - \bar{x}_2)/(s_p^2/4)^{1/2} < -t_{.05,14} = -1.761, \qquad (3\text{-}4)$$

where the pooled sample variance was

$$s_p^2 = (s_1^2 + s_2^2)/2. \qquad (3\text{-}5)$$

Fulfillment of the condition stated in (3-4) required rejection of the null hypothesis that the population means are equal. In such a case, the evidence supported acceptance of the alternate hypothesis that the independent variable under consideration has a significant effect on the dependent variable. Since the sample sizes were equal, the test statistic had Student's t distribution even if the variances of the sample populations were unequal [69, p. 294]; the F-test for equality of population variances was not required. The hypothesized dependence of bubble column interfacial area per unit volume on absorbent solution composition, especially acid (strong electrolyte) content, was also evaluated through the use of the small-sample t-test for equality of population means.

The model chosen for determination of pollutant reduction parameter R_h dependence on y_{ps}, C_{1a}, and C_{1h} for NO_x was

$$R_h = ky_{ps}^{\alpha}C_{1a}^{\beta}C_{1h}^{\gamma}. \tag{3-6}$$

Similarly, the premise that pollutant removal rates were primarily dependent on solubility of the pollutant in water was evaluated using the model

$$R_h = kH_p^{\alpha}. \tag{3-7}$$

A good fit of the experimental data to this model would be sufficient evidence to conclude that the effect of pollutant solubility on absorption rate dominates any concentration-dependent effects (y_{ps}, C_{1a}, or C_{1h}).

Correlation of the data with these models was found by performing linear regressions on their logarithmic forms. For example, the logarithmic form of (3-8),

$$\ln R_h = \ln k + \alpha \ln H_p, \tag{3-8}$$

was fit to the data via a simple linear regression. Extension of the least-squares calculations [69, p. 484] to 3 dependent variables was required for the logarithmic form of (3-6),

$$\ln R_h = \ln k + \alpha \ln y_{ps} + \beta \ln C_{1a} + \gamma \ln C_{1h}. \tag{3-9}$$

For this forms, the geometric mean NO_x runs of Figure 6 and Table 3 became arithmetic means of the extrema.

Finally, the "goodness-of-fit" of these models to the experimental data was evaluated using the coefficient of determination [69, p. 503]

$$r^2 = 1 - [\Sigma(y - y')^2/\Sigma(y - \bar{y})^2]. \tag{3-10}$$

This statistical parameter is the fraction of total sample variance explained by the model being tested. A value of zero indicates total lack of fit of the model to the data, while a value of unity indicates perfect fit.

CHAPTER FOUR
DATA AND RESULTS

Column Physical Behavior

Mass transfer between a gas and a liquid must occur through the two-phase interface created by gas-liquid contact. The greater the interfacial area of contact, the more rapid will be the transfer of mass between the two phases. Since a major purpose of any separation process is to effect the desired rate of mass transfer in the least volume, the primary physical performance parameter for gas-liquid contact is the interfacial area per unit volume.

To determine this interfacial area, the physical behavior of the bubble column used in this study was carefully observed. The same sparger, gas flow rate, column diameter, and liquid temperature were used for all process experimental runs. Stable movement patterns of spherical bubbles were produced, and no backmixing of bubbles was observed. The type of pollutant (SO_2, CO, NO, or NO_2) and its concentration in the gas had no observable effect on bubble diameter or movement. The only independent variables which appeared to cause changes in bubble diameter, number density, or movement pattern were those of liquid composition.

The effects of liquid composition on bubble column physical characteristics are presented in Table 4. Variation in acid type and acid or H_2O_2 concentrations produced little change in column height, volume, or gas holdup. Variation of gas-liquid interfacial area per unit volume

TABLE 4. Effects of Liquid Composition on Bubble Column Physical Behavior.

ACID	C_{1a} (gmol/1)	C_{1h} (gmol/1)	h_c (cm)	V_c (cm^3)	v_g[a] -	d_b (cm)	a (1/cm)[b]
H_2SO_4	0.4	0.5	40.5	121.5	0.054	0.4	0.8
H_2SO_4	0.4	5.0	40.6	122.0	0.057	0.4	0.9
H_2SO_4	4.0	0.5	40.4	121.0	0.050	0.2	1.5
H_2SO_4	4.0	5.0	40.5	121.5	0.054	0.2	1.6
HNO_3	0.4	0.5	40.5	121.5	0.054	0.3	1.1
HNO_3	0.4	5.0	40.7	121.5	0.061	0.3	1.2
HNO_3	4.0	0.5	40.8	123.0	0.065	0.1	3.9
HNO_3	4.0	5.0	40.9	123.5	0.069	0.05	8.3

[a] $V_1 = 115\ cm^3$ for all entries and $v_g = 1 - (V_1/V_c)$.

[b] Interfacial area parameter has the unreduced units cm^2/cm^3.

was almost solely due to changes in bubble size and therefore number density.

Results of statistical tests of the dependence of column interfacial area per unit volume on liquid composition are shown in Table 5. At the 95 percent confidence level, the evidence clearly supports the premise of interfacial area dependence on acid type and concentration.

The evidence was insufficient to reject the null hypothesis for H_2O_2 concentration dependence. However, since close examination of the data in Table 4 reveals increased interfacial area for increased H_2O_2 concentration in all cases, it is quite possible that a larger sample size would have resulted in acceptance of the hypothesized dependence of interfacial area on H_2O_2 concentration.

At high HNO_3 concentration, the interfacial area parameter was quite sensitive to variation in H_2O_2 concentration. Evidently, some synergistic interaction between HNO_3 and H_2O_2 was taking place. The author was unable to discern the causal mechanism for this interaction.

Process Startup Transients

Initial transient behavior of the experimental bubble column was characterized by the time after initiation of pollutant gas flow required for steady state to be reached. As derived in Appendix B, this time interval $(t_c)_{max}$ is inversely proportional to the solubility parameter H_p. Due to its wide range of values for the gases studied, the solubility parameter greatly effected the time constants for column startup transients.

TABLE 5. Effects of Liquid Composition on Interfacial Area Parameter.

SAMPLES		STATISTICS[a]					DECISION[b]
1	2	$\bar{x}_1$	$\bar{x}_2$	s_1	s_2	t	t < 1.761 ?
H_2SO_4	HNO_3	1.200	3.625	0.378	3.125	-2.179	YES
$C_{1a} = 0.4$	$C_{1a} = 4.0$	1.000	3.825	0.169	2.947	-2.707	YES
$C_{1h} = 0.5$	$C_{1h} = 5.0$	1.825	3.000	1.308	3.282	-0.941	NO

[a] Statistical quantities in this table have the units cm^2/cm^3 or 1/cm.

[b] With a 95% confidence level and 8 data points per sample, the 2-sample statistic for test of equality of population means is $-t_{.05,14} = -1.761$.

As shown in Table 6, calculated values for this time interval varied from about 4 sec for CO to 5.6 min for low SO_2 concentration into the bubble column. During each experimental run, pollutant samples were taken at 10, 15, and 20 min after gas flow was initiated. Although measured pollutant concentrations in the samples varied by as much as ±10 percent of their average valve for each run, no pattern of increase or decrease in the measured values for each run was discernible. Pollutant concentration determination was therefore never compromised by sampling during the period of unsteady-state behavior.

Process Steady-State Behavior

Sulfur Dioxide

Results for all SO_2 experiments are displayed in Table 7. The absorption of SO_2 into H_2O_2 solutions acidified with H_2SO_4 was so rapid that there was no detectable pollutant in the column effluent for any of the experimental runs. This result prompted recalibration of the SO_2 detector tubes; no discernible error was found. Early sampling of effluent from an identically sized column of pure water was then accomplished; equilibration time was found to be about 4 min. Therefore, an unexpectedly long startup transient was eliminated as an explanation for the remarkable performance of the small SO_2 bubble column.

Carbon Monoxide

In contrast to the SO_2 process, absorption of CO into acidified H_2O_2 solutions was extremely slow (see Tables 8 and 9). For two of the experimental runs, negative removal rates were calculated. This is

TABLE 6. Time Constants for Column Startup Transients.

GAS	V_l (cm^3)	H_p[a] (atm-l/gmol)	t_c (sec)	$5t_c$ (min)
CO	115	1370	0.82	0.068
NO_x	50	585	0.84	0.070
NO_x	115	585	1.92	0.160
NO_x	180	585	3.01	0.251
CO_2	115	50.9	22.1	1.84
SO_2[b]	3	0.504	58.7	4.89
SO_2[c]	3	0.442	66.7	5.56

[a] H_p values from Table 2 except for NO_x; H_p for NO_x is the average of NO and NO_2 values.

[b] H_p for y_{ps} = 1000 ppm.

[c] H_p for y_{ps} = 100 ppm.

TABLE 7. Absorption of SO_2 into H_2SO_4-H_2O_2 Solutions.

Y_{ps} (ppm)	C_{la} (gmol/l)	C_{lh} (gmol/l)	Y_{pf} (ppm)	R_h[a] (%/cm)
100	0.4	0.5	≤ 1[b]	≥ 99
100	0.4	5.0	≤ 1	≥ 99
100	4.0	0.5	≤ 1	≥ 99
100	4.0	5.0	≤ 1	≥ 99
1000	0.4	0.5	≤ 1	≥ 99
1000	0.4	5.0	≤ 1	≥ 99
1000	4.0	0.5	≤ 1	≥ 99
1000	4.0	5.0	≤ 1	≥ 99

[a] $V_l = 3$ cm^3 and $h_c = 1$ cm.

[b] Below detection limit (1 ppm).

TABLE 8. Absorption of CO into H_2SO_4-H_2O_2 Solutions.

y_{ps} (ppm)	C_{1a} (gmol/1)	C_{1h} (gmol/1)	a (1/cm)	P_{vf} (atm)	y_{pf} (ppm)	$F_p \times 10^{11}$ (gmol/min-cm^3)	R_h (%/cm)
200	0.4	0.5	0.81	0.033	193	-22.9	-0.0556
200	0.4	5.0	0.86	0.034	187	6.6	0.0160
200	4.0	0.5	1.5	0.034	188	2.3	0.0055
200	4.0	5.0	1.6	0.033	185	16.3	0.0397
2000	0.4	0.5	0.81	0.031	1885	-21.8	-0.0053
2000	0.4	5.0	0.86	0.031	1834	252.	0.0615
2000	4.0	0.5	1.5	0.030	1840	256.	0.0624
2000	4.0	5.0	1.6	0.027	1840	325.	0.0792

TABLE 9. Absorption of CO into HNO_3-H_2O_2 Solutions.

y_{ps} (ppm)	C_{1a} (gmol/l)	C_{1h} (gmol/l)	a (1/cm)	P_{vf} (atm)	y_{pf} (ppm)	$F_p \times 10^{11}$ (gmol/min-cm^3)	R_h (%/cm)
200	0.4	0.5	1.1	0.033	186	12.3	0.0299
200	0.4	5.0	1.2	0.032	185	15.6	0.0383
200	4.0	0.5	3.9	0.032	184	23.4	0.0572
200	4.0	5.0	8.3	0.032	183	31.4	0.0769
2000	0.4	0.5	1.1	0.027	1851	239.	0.0583
2000	0.4	5.0	1.2	0.028	1838	298.	0.0729
2000	4.0	0.5	3.9	0.028	1833	309.	0.0759
2000	4.0	5.0	8.3	0.029	1812	415.	0.102

indicative of some error in the analytical technique, not net production of CO in the bubble column.

The statistical tests for dependence of pollutant removal F_p per unit column volume for CO are presented in Table 10. The hypothesized dependence of F_p on pollutant inlet concentration y_{ps} is acceptable at the 95% confidence level. However, the premise that F_p is dependent on liquid composition is not supported by the data.

This unfortunately appears to be an artifact of the experimental design. The differences in F_p values for low and high y_{ps} are so great that partitioning the data any other way always produces a bimodal distribution. The sample variances for these distributions are so large that the effects of independent variables other than y_{ps} are masked.

Such is not the case for the percent pollutant removal R_h per unit column height. Since this performance parameter is a ratio of y_p values, its use in this case eliminates bimodal distributions of data for independent variables other than y_{ps}.

The statistical tests of R_h dependence on pollutant concentration and liquid composition for CO are presented in Table 11. The dependence of R_h on y_{ps} and on acid type and concentration is clearly supported by the data. However, R_h dependence on H_2O_2 concentration is inconclusive. As in the results for the interfacial area parameter, a larger sample size might have revealed the dependence of R_h on H_2O_2 concentration. On this basis, CO percent removal efficiency had the same ordinal dependence on liquid composition as did the interfacial area per unit of bubble column volume.

TABLE 10. Effects of Gas and Liquid Compositions of F_p for CO Absorption.

SAMPLES		STATISTICS[a]					DECISION[b]
1	2	$\bar{x}_1$	$\bar{x}_2$	s_1	s_2	t	$t < 1.761$?
$y_{ps} = 200$	$y_{ps} = 2000$	10.6	259.0	16.3	126.5	-5.508	YES
H_2SO_4	HNO_3	101.7	168.0	148.0	164.7	-0.847	NO
$C_{1a} = 0.4$	$C_{1a} = 4.0$	97.4	172.3	138.9	170.4	-0.964	NO
$C_{1h} = 0.5$	$C_{1h} = 5.0$	99.7	170.0	141.6	169.3	-0.900	NO

[a] Statistical quantities in this table have the units (gmol/min-cm^3) x 10^{-11}.

[b] With a 95% confidence level and 8 data points per sample, the 2-sample statistic for test of the equality of population means is $-t_{.05,14} = -1.761$.

TABLE 11. Effects of Gas and Liquid Composition on R_h for CO Absorption.

SAMPLES		STATISTICS[a]					DECISION[b]
1	2	$\bar{x}_1$	$\bar{x}_2$	s_1	s_2	t	t < 1.761 ?
$y_{ps} = 200$	$y_{ps} = 2000$	0.0260	0.0634	0.0398	0.0310	-2.097	YES
H_2SO_4	HNO_3	0.0254	0.0639	0.0443	0.0231	-2.180	YES
$C_{1a} = 0.4$	$C_{1a} = 4.0$	0.0270	0.0624	0.0421	0.0293	-1.952	YES
$C_{1h} = 0.5$	$C_{1h} = 5.0$	0.0285	0.0608	0.0445	0.0278	-1.741	NO

[a] Statistical quantities in this table have the units %/cm.

[b] With a 95% confidence level and 8 data points per sample, the 2-sample statistic for test of the equality of population means is $-t_{.05,14} = 1.761$.

Nitrogen Oxides

Data for absorption of NO and NO_2 into HNO_3-H_2O_2 solutions are presented in Table 12. The first 5 runs were made with pollutant-free gas. Reaction between H_2O_2 and HNO_3 produced NO_2 in the column effluent, especially when both were in high concentration in the liquid.

Varying levels of NO_2 were found in the effluent from NO absorption. Levels of NO_2 higher than those found with pollutant-free gas indicate that some NO was being converted to NO_2 in the bubble column. No production of NO was detected during the NO_2 runs.

For every combination of y_{ps}, C_{1a}, and C_{1h}, NO_2 was more rapidly absorbed than NO. Also, NO_2 levels were lower than NO levels in the effluent from all NO absorption runs. Therefore, for any combination of NO and NO_2, the percentage rates of removal will always be less for NO than for NO_2. Consequently, the NO rates were taken to be the limiting minimum rates for NO_x (NO + NO_2).

A correlation of R_h values for NO with y_{ps}, C_{1a}, and C_{1h} is presented in Table 13. As in the cases for the interfacial area parameter and R_h for CO absorption, acid concentration had the greatest effect (largest exponent in the correlation). However, the dependence of R_h for NO on H_2O_2 concentration was almost as large as its dependence on the pollutant inlet concentration. Since this model accounts for only 43.6 percent of the total variance in the data, it is possible that some other empirical relationship linking R_h and y_{ps}, C_{1a}, and C_{1h} for NO might fit the data better.

TABLE 12. Absorption of NO_x into HNO_3-H_2O_2 Solutions.

y_{ps} (ppm)	C_{la} (gmol/l)	C_{lh} (gmol/l)	a (1/cm)	INPUT GAS	y_{pf}(ppm)	
					NO	NO_2
0	0.4	0.5	1.1	Zero	<1[a]	1
0	0.4	5.0	1.2	Zero	<1	2
0	1.26	1.58	1.8	Zero	<1	3
0	4.0	0.5	3.9	Zero	<1	6
0	4.0	5.0	8.3	Zero	<1	28
100	0.4	0.5	1.2	NO	93	5
100	0.4	0.5	1.2	NO_2	<1	86
100	0.4	5.0	1.3	NO	79	9
100	0.4	5.0	1.3	NO_2	<1	66
100	4.0	0.5	4.4	NO	60	12
100	4.0	0.5	4.4	NO_2	<1	55
100	4.0	5.0	10.0	NO	44	38
100	4.0	5.0	10.0	NO_2	<1	43
316	1.26	1.58	1.8	NO	200	8
316	1.26	1.58	1.8	NO_2	<1	96
1000	0.4	0.5	0.85	NO	550	4
1000	0.4	0.5	0.85	NO_2	<1	260
1000	0.4	5.0	0.91	NO	490	18
1000	0.4	5.0	0.91	NO_2	<1	235
1000	4.0	0.5	3.2	NO	335	16
1000	4.0	0.5	3.2	NO_2	<1	80
1000	4.0	5.0	7.0	NO	195	84
1000	4.0	5.0	7.0	NO_2	<1	53

[a] Below detection limit.

TABLE 13. Limiting Absorption Rates for NO_x into HNO_3-H_2O_2 Solutions

y_{ps} (ppm)	C_{1a} (gmol/l)	C_{1h} (gmol/l)	h_c[a] (cm)	P_{vf} (atm)	y_{pf} (ppm)	R_h[b] (%/cm)	R_h[c] (%/cm)	Error[d] (%)
100	0.4	0.5	17.4	0.029	93	0.01	0.13	1200
100	0.4	5.0	17.5	0.030	79	0.86	0.21	-76
100	4.0	0.5	17.6	0.033	60	2.00	0.81	-59
100	4.0	5.0	17.7	0.031	44	2.97	1.38	-53
316	1.26	1.58	40.7	0.032	200	0.81	0.57	-30
1000	0.4	0.5	63.2	0.032	550	0.68	0.24	-65
1000	0.4	5.0	63.3	0.032	490	0.77	0.41	-47
1000	4.0	0.5	63.6	0.033	335	1.02	1.54	51
1000	4.0	5.0	63.8	0.032	195	1.25	2.61	109

[a] Column height was varied to keep pollutant sampled concentrations within detection range.

[b] Limiting R_h values are for NO, since it is absorbed at a slower rate than NO_2 (see Table 12).

[c] Correlation $R_h = 0.86 y_{ps}^{0.279} C_{1a}^{0.807} C_{1h}^{0.229}$, $r^2 = 0.436$, $n = 9$.

[d] Error = 100(Correlation R_h - Limiting R_h)/Limiting R_h.

Solubility Dependence of Absorption Rate

To test the premise that, of all the independent variables in the process model, pollutant absorption rate is primarily dependent on its solubility in aqueous solutions, a simple correlation between R_h and H_p was performed. As shown in Table 14, percent removal R_h per unit column height was found to be directly proportional to pollutant solubility (inversely proportional to H_p). This model fits the data quite well, accounting for 86.5 percent of the total variance; the variance due to experimental error, averaging of R_h values for each gas, and all other independent variables (y_{ps}, C_{1a}, and C_{1h}) accounts for only 13.5 percent of the total variance.

TABLE 14. Correlation of Average R_h with H_p for CO, NO, and SO_2.

GAS	H_p[a] (atm/l-gmol)	R_h[b] (%/cm)	R_h[c] (%/cm)	Error[d] (%)
CO	1370	0.0554	0.0974	76
NO	700	1.15	0.176	-85
SO_2[e]	0.457	99.	110.	11

[a] Values of H_p from Table 2.

[b] Average of R_h values in Tables 8 and 9 (CO), 13 (NO), and 7 (SO_2); for SO_2, $R_h \geq 99$, but $R_h = 99$ is assumed for the purpose of this correlation.

[c] Correlation $R_h = 55.3H_p^{-0.878}$, $r^2 = 0.865$, $n = 31$. Values of R_h for all experimental runs used in determination of this correlation.

[d] Error = 100(Correlation R_h - Average R_h)/Average R_h.

[e] Value of H_p for SO_2 at $y_{ps} = 316$ ppm (geometric mean of experimental y_{ps} values 100 ppm and 1000 ppm).

CHAPTER FIVE
CONCLUSIONS AND RECOMMENDATIONS

Comparison of Theory and Results

The rates of absorption of the gaseous pollutants SO_2, CO, and NO_x into acidified H_2O_2 solutions in a bubble column were hypothesized to be limited by diffusion in the liquid interphase region. The resultant process model predicted that the molar rate F_p of pollutant absorption per unit bubble column volume would be directly proportional to the gas-liquid interfacial area per unit volume, the pollutant gas-phase concentration, and the solubility of pollutant in aqueous solution. Interfacial area was predicted to be primarily dependent on acid concentration in the liquid, with little dependence on H_2O_2 concentration.

For the bubble column used in this study, interfacial area per unit column volume was shown to be dependent on the solution acid type as well as the acid concentration. For equal molar concentrations, HNO_3 increased the interfacial area more than H_2SO_4; greater acid concentration, regardless of type, also caused increased interfacial area.

The data was insufficient to support the premise that the interfacial area parameter is dependent on H_2O_2 concentration in acidified solution. However, the interfacial area was sensitive to variation in H_2O_2 concentration at high concentrations of HNO_3. The mechanism for this synergistic interaction was not determined.

Based on CO absorption data, the pollutant molar absorption rate F_p per unit column volume was shown to be dependent on the gas-phase pollutant concentration y_{ps}; increased y_{ps} caused more rapid absorption. However, the strong dependence of F_p on y_{ps} statistically masked its dependence on other process variables. For the experimental design used in this study, F_p was not very suitable as a measure of process dynamics.

The percentage rate R_h of pollutant removal per unit bubble column height was shown to be dependent not only on the pollutant concentration y_{ps} but also on the liquid composition. Based on CO absorption data, R_h valves were higher with HNO_3 than with H_2SO_4 as the acid component of the bubble column liquid. Also, R_h positively correlated with acid concentration, regardless of acid type.

Both R_h and the interfacial area parameter showed the same ordinal dependence on liquid composition. This evidence thus supports the basic premise that the pollutant absorption rate per unit bubble column volume or height is roughly proportional to the gas-liquid interfacial area.

The overall dependence of R_h on pollutant solubility in aqueous solution was shown to be unequivocal. Highly soluble SO_2 was absorbed very rapidly into acidified H_2O_2 solutions, NO at a much slower rate (with some conversion to NO_2), and sparingly soluble CO negligibly so.

In summary, rate of absorption of pollutant into acidified hydrogen peroxide solutions is positively correlated with gas-phase concentration of the pollutant, gas-liquid interfacial area, and solubility of the pollutant in the aqueous absorbent liquid. It can thus be concluded, in accordance with the assumptions on which the now-validated process model was based, that the rate of absorption in the subject process is limited by diffusion in the liquid-side interphase region, at least for a sparingly soluble pollutant, such as CO, at low concentrations in the gas phase.

Practicality of the Process

The percentage removal efficiency R_h per unit bubble column height is a suitable performance parameter for practical evaluation of this absorption process. Given a combustion waste-gas stream with pollutant concentration y_{ps} and a desired effluent concentration limit y_{pf}, the concentration reduction ratio for the process is related to the average R_h for a given pollutant (for an experimental data set as shown in Figure 6 of Chapter 3) and to the column fluid height h_c by

$$y_{pf}/y_{ps} = [1 - (R_h/100)]h_c. \qquad (5\text{-}1)$$

The fluid height of the bubble column required to effect the desired concentration reduction ratio is then

$$h_c = \ln(y_{pf}/y_{ps})/\ln[1 - (R_h/100)] \qquad (5\text{-}2)$$

Although an actual staged absorption column would be taller than the fluid height (due to interstage sparger structure and voids), h_c can be used to compare the effectiveness of this process for the pollutants of interest.

Results of h_c calculations for 99% reduction in pollutant concentration for SO_2, NO_x, and CO are presented in Table 15. The very rapid absorption and reaction of SO_2 with acidified H_2O_2 solutions means that this process is imminently suitable for removal of SO_2 and production of H_2SO_4 from waste-gas streams. The exceedingly tall column required for

TABLE 15. Column Height for 99% Reduction in Pollutant Concentration.

POLLUTANT GAS	R_h[a] (%/cm)	h_c[b] (cm)
SO_2	99.	1
NO_x	1.15	398
CO	0.0554	8310

[a] Average experiment values (from Table 14).

[b] Fluid height only (see text).

99% CO reduction would make this process unsuitable for removal of CO from gas streams.

The ratio of fluid column heights for NO_x and SO_2 is about 400 to 1 respectively. This ratio is sufficiently large to allow sequential removal of SO_2 and NO_x from a polluted gas stream (see Figure 7). Separate solutions of nearly pure sulfuric and nitric acids could be produced in this manner. By its very nature, the process of SO_2-NO_x absorption into acidified H_2O_2 solutions would act as a separation process for the product sulfuric and nitric acids.

The Next Step

In order to develop this sequential process for large-scale industrial and life-support applications, it must be studied at the pilot-plant scale. Several different gas-liquid contact devices would have to be evaluated to determine the device that would minimize column size (height and diameter) for reasonable gas-stream pressure drop.

In addition to staged bubble-column devices (sieve-tray and bubble-cap towers), a packed-bed tower should be evaluated. Evidence presented by Deckwer and Hallensleben [66] suggests that the maximal rate of interfacial mass transfer occurs during formation of the gas-liquid interface. A packed bed would cause continual destruction and reformation of the interface as liquid trickled down through the packing. This might result in a higher average mass-transfer rate than could be achieved in staged bubble devices, even with very short stages.

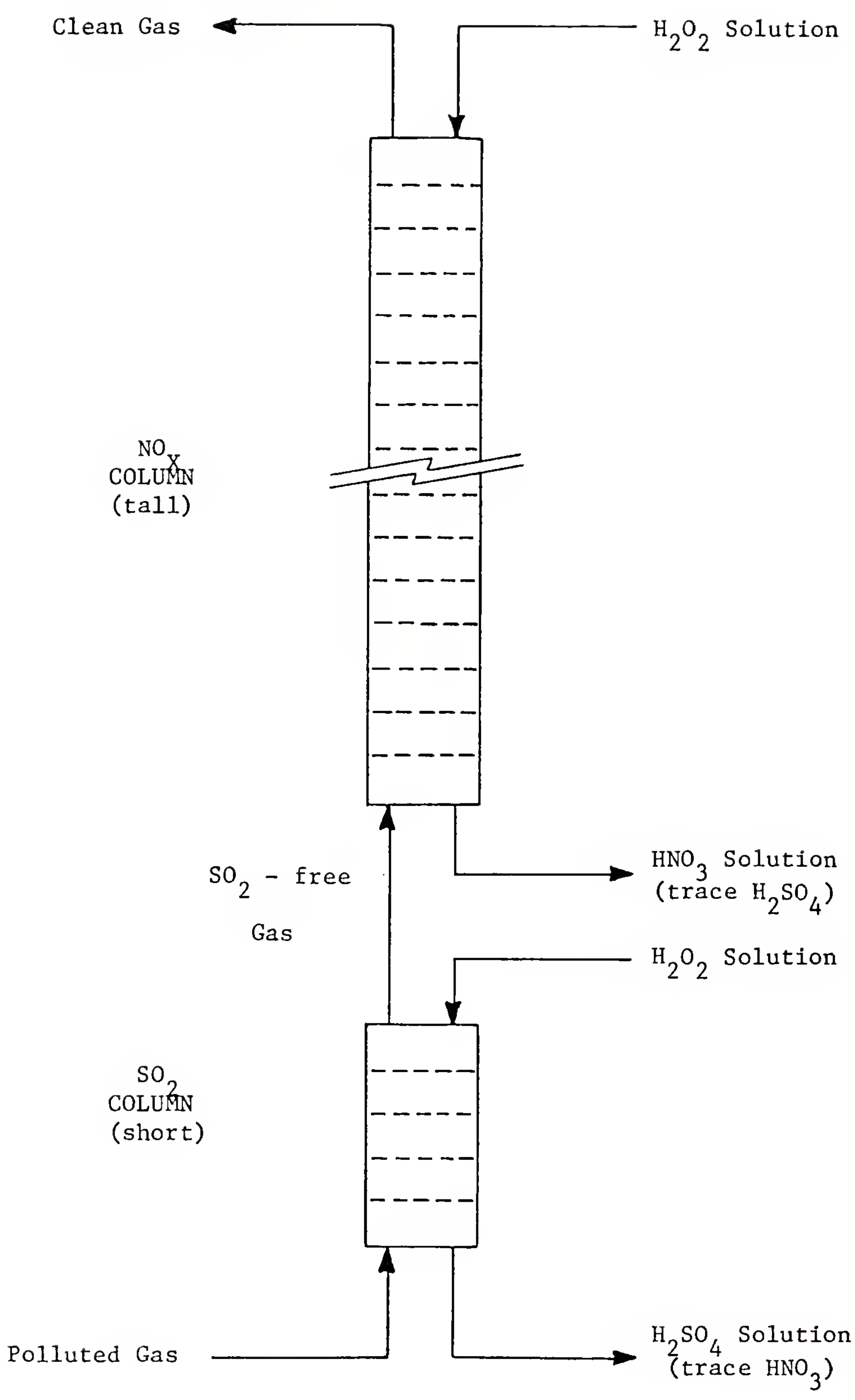

FIGURE 7. Sequential Absorption of SO_2 and NO_X from a Gas Stream.

Finally, the effects of column temperature and pressure should be studied to determine the absorption conditions that would minimize column size within reasonable structural and materials constraints.

A New Paradigm

The basic idea for large-scale application of the subject process was conceived by the author of this study after he learned of its use for quantitative determination of sulfur and nitrogen oxides in air and stack gases. Ruch [70, 71] has compiled bibliographies of several thousand techniques for quantitative analysis of hundreds of different toxic gaseous substances in air. Surely some of these techniques would have practical large-scale application in industry and in closed environments.

In general, systematic evaluation of analytical chemical separation techniques for use as industrial-scale separation processes might help improve the quality of life for us all.

REFERENCES

1. G. K. O'Neill. "The High Frontier: Human Colonies in Space." Bantam, New York, 1978.

2. G. H. Stine. "The Third Industrial Revolution." G. P. Putnam's Sons, New York, 1975.

3. S. Ostrach. Convective phenomena of importance for materials processing in space. In "Materials Sciences in Space with Applications to Space Processing." Vol. 52, Progress in Astronautics and Aeronautics, AIAA, New York, 1977.

4. P. E. Glaser. Solar Power from satellites. Physics Today 30(2):30 (1977).

5. P. E. Glaser. The Earth benefits of solar power satellites. Space Solar Power Review 1(1):9(1980).

6. D. L. Kuck. Near-Earth extraterrestrial resources. In "Space Manufacturing Facilities III. " AIAA, New York, 1979.

7. D. R. Criswell and R. E. Waldron. Commercial prospects for extraterrestrial materials. J. Contemporary Business 7:153(1978).

8. B. Z. Henry and C. H. Eldred. Advanced technology and future Earth-to-orbit transportation systems. In "Space Manufacturing Systems II." AIAA, New York, 1977.

9. H. Kolm and G. K. O'Neill. Mass-drivers for lunar materials transport and as reaction engines. In "Proceedings, 1977 IAF Conference on Astronautics." International Astronautics Federation, Prague, 1977.

10. J. P. Layton. Propulsion options for orbital transfers in cislunar space. In "Space Manufacturing Facilities II. " AIAA, New York, 1977.

11. R. E. Waldron, F. Erstfeld, and D. R. Criswell. The role of chemical engineering in space manufacturing. Chemical Engineering 86(4):80(1979).

12. R. H. Miller and D. B. S. Smith. "Extraterrestrial Processing and Manufacturing of Large Space Systems: Executive Summary." Vol. III, NASA CR-161293, 1979.

13. G. K. O'Neill. The low (profile) road to space manufacturing. Astronautics and Aeronautics 16(3):24(1978).

14. J. P. Vajk, J. H. Engel, and J. A. Shettler. Habitat and logistic support requirements for the initiation of a space manufacturing enterprise. In "Space Resources and Space Settlements." NASA SP-428, 1979.

15. B. Parkinson. Small high-technology communities on the Moon. Spaceflight 19(2):42 (1977).

16. E. Crawley. Designing the space colony. Technology Review 79(8):44 (1977).

17. R. Salkeld. Impact of advanced space transportation on terrestrial, lunar, and asteroidal materials costs. In "Space Manufacturing Facilities III. " AIAA, New York, 1979.

18. J. Spurlock and M. Modell. Systems engineering overview for regenerative life-support systems applicable to space habitats. In "Space Resources and Space Settlements." NASA SP-428, 1979.

19. J. M. Phillips. Controlled-environment agriculture and food production systems for space manufacturing. In "Space Manufacturing Facilities II." AIAA, New York, 1977.

20. M. R. Fontes. Controlled-environment horticulture in the Arabian Desert at Abu Dhabi. HortScience 8:13 (1973).

21. J. Spurlock, M. Modell, D. F. Putnam, L. W. Ross, and J. N. Pecocaro. "Evaluation and Comparison of Alternative Designs for Spacecraft Water/Solid-Waste Processing Systems." Final Report, NASA Contract NASW-2439, 1975.

22. M. Modell. Sustaining life in a space colony. Technology Review 79(8):36 (1977).

23. E. Aurbach and S. Russell. New approaches to contaminant control in spacecraft. In "Atmosphere in Space Cabins and Closed Environments." Meredith, New York, 1966.

24. W. R. Niessen. "Combustion and Incineration Processes." Marcel Dekker, New York, 1978.

25. J. H. Seinheld. "Air Pollution: Physical and Chemical Fundamentals." McGraw-Hill, New York, 1975.

26. A. Phillips. The modern sulfuric acid process. In "The Modern Inorganic Chemicals Industry." The Chemical Society, London, 1977.

27. S. P. S. Andrew. Modern processes for the production of ammonia and nitric acid. In "The Modern Inorganic Chemicals Industry." The Chemical Society, London, 1977.

28. A. P. Altshuller and J. J. Bufalini. Photochemical aspects of air pollution--A critical review. Environmental Science and Technology 5:30 (1971).

29. H. Babich, D. L. Davis, and G. Stotsky. Acid precipitation--causes and consequences. Environment 22(4):6 (1980).

30. H. C. Perkins. "Air Pollution." McGraw-Hill, New York, 1974.

31. B. G. Ferris. Health effects of exposure to low levels of regulated air pollutants--A critical review. J. Air Pollution Control Assoc. 28:483 (1978).

32. W. G. Lloyd and D. R. Rowe. Homogeneous catalytic oxidation of carbon monoxide. Environmental Science and Technology 5:1133 (1971).

33. S. J. Biondo and J. C. Marten. A history of flue gas desulfurization systems. J. Air Pollution Control Assoc. 27:948 (1977).

34. R. F. Vogel, B. R. Mitchell, and F. E. Massoth. Reactivity of sulfur dioxide and supported metal-oxide/alumina sorbents. Environmental Science and Technology 8:433 (1974).

35. F. Johswich. Removal of sulfur and nitrogen oxides. U. S. Patent 3,502,427 (1970).

36. I. J. James. Separation of mixtures of nitrogen oxides on activated carbon column. U. S. Patent 2,568,396 (1951).

37. B. B. Sundaresan, C. I. Harding, F. P. May, and E. R. Hendrickson. Adsorption of nitrogen oxides from waste gas. Environmental Science and Technology 1:151 (1967).

38. H. Kobayashi, N. Takezawa, and T. Niki. Removal of nitrogen oxides with aqueous solutions of inorganic and organic reagents. Environmental Science and Technology 11:191 (1977).

39. C. A. Crampton, G. Faber, R. Jones, J. P. Leaver, and S. Schelle. The manufacture, properties, and uses of hydrogen peroxide. In "The Modern Inorganic Chemicals Industry." The Chemical Society, London, 1977.

40. F. A. Lowenheim and M. K. Moran. "Industrial Chemicals," 4th Edition. Wiley-Interscience, New York, 1975.

41. American Public Health Association, Inc. "Methods of Air Sampling and Analysis," 2nd. Edition. APHA, Washington, 1977.

42. P. Thirion. Method for purification of industrial flue gases. U. S. Patent 3,953,578 (1976).

43. P. V. Danckwerts. "Gas-Liquid Reactions." McGraw-Hill, New York, 1970.

44. T. K. Sherwood, R. L. Pigford, and C. R. Wilke. "Mass Transfer." McGraw-Hill, New York, 1975.

45. R. E. Treybal. "Mass-Transfer Operations." McGraw-Hill, New York, 1980.

46. W. G. Whitman. Preliminary experimental confirmation of the film theory of gas absorption. Chem. and Metal. Engng. 29(4):147 (1923).

47. R. Higbie. The rate of absorption of a pure gas into a still liquid during short periods of exposure. Trans. Amer. Inst. Chem. Engrs. 31:365 (1935).

48. P. V. Danckwerts. Significance of liquid-film coefficients in gas absorption. Ind. and Engng. Chem. 43:1460 (1951).

49. C. J. King. Turbulent liquid-phase mass transfer at a free gas-liquid interface. Ind. and Engng. Chem. Fund. 5:1 (1966).

50. W. K. Lewis and W. G. Whitman. Principles of gas absorption. Ind. and Engng. Chem. 16:1215 (1924).

51. W. L. McCabe and J. C. Smith. "Unit Operations of Chemical Engineering." McGraw-Hill, New York, 1976.

52. J. R. Welty, C. E. Wicks, and R. E. Wilson. "Fundamentals of Momentum, Heat, and Mass Transfer." Wiley, New York, 1969.

53. E. L. Cussler. "Multicomponent Diffusion." Chemical Engineering Monograph 3, Elsevier, New York, 1976.

54. G. Marrucci and L. Nicodemo. Coalescence of gas bubbles in aqueous solutions of inorganic electrolytes. Chem. Engng. Science 22:1257 (1967).

55. J. Voight and K. Schugerl. Absorption of oxygen in multistage bubble columns. Chem. Engng. Science 34:1221 (1979).

56. J. Halperin and H. Taube. The reaction of hydrogen peroxide with sulfite and thiosulfate. J. Amer. Chem. Soc. 74:380 (1952).

57. E. Halfpenny and P. L. Robinson. The reaction between hydrogen peroxide and pernitrous acid. J. Chem. Soc. 1952:928.

58. G. Margolis and J. N. Driscoll. Rate-controlling processes in manual determination of nitrogen oxides in flue gases. Environmental Science and Technology 6:727 (1972).

59. D. S. Mehta and S. Calvert. Gas sorption by suspensions of activated carbon in water. Environmental Science and Technology 1:325 (1967).

60. W. C. Schumb, C. N. Satterfield, and R. L. Wentworth. "Hydrogen Peroxide," American Chemical Society Monograph Series. Reinhold, New York, 1955.

61. W. H. Hatcher and D. W. MacLauchlan. Conductivity of aqueous mixtures of hydrogen peroxide and nitric acid. Canadian J. of Research 16B(8):253 (1938).

62. R. C. Reid, J. M. Prausnitz, and T. K. Sherwood. "The Properties of Gases and Liquids," 3rd. Edition. McGraw-Hill, New York, 1977.

63. Metcalf and Eddy, Inc. "Wastewater Engineering: Treatment, Disposal, Reuse." McGraw-Hill, New York, 1979.

64. R. H. Perry and C. H. Chilton. "Chemical Engineers' Handbook," 5th Edition. McGraw-Hill, New York, 1973.

65. E. R. Kuczynski. Effects of gaseous air pollutants on the response of the Thomas SO_2 Autometer. Environmental Science and Technology 1:68 (1967).

66. W. D. Deckwer and J. Hallensleben. Gas sparger influence on mass transfer in bubble columns. Canadian J. of Chem. Engng. 58:190 (1980).

67. S. G. Wechter. Preparation of stable pollution gas standards. In "Calibration in Air Monitoring." American Society for Testing and Materials, Philadelphia, 1976.

68. G. S. Samuelson and J. H. Harman. Chemical transformations of nitrogen oxides while sampling combustion product. J. Air Pollution Control Assoc. 27:648 (1977).

69. J. T. McClave and T. H. Dietrich. "Statistics." Dellen, San Francisco, 1979.

70. W. E. Ruch. "Chemical Detection of Gaseous Pollutants: An Annotated Bibliography." Ann Arbor Science, Ann Arbor, 1966.

71. W. E. Ruch. "Quantitative Analysis of Gaseous Pollutants." Humphrey, Ann Arbor, 1970.

APPENDIX A
DERIVATION OF DATA REDUCTION EQUATIONS

The molar rate of pollutant absorbed in a unit volume of a bubble column is

$$F_p = (\dot{N}_{pi} - \dot{N}_{po})/V_c. \tag{A-1}$$

The molar flow rate of pollutant is related to its gas-phase concentration and gas flow rate by

$$\dot{N}_p = C_{gp}G. \tag{A-2}$$

Then

$$F_p = (C_{gpi}G_i - C_{gpo}G_o)/V_c. \tag{A-3}$$

Upstream and downstream of an absorption column, pollutant mass and mole number are conserved. In this study, column inlet conditions were related to the controlled upstream dry-gas standard conditions via the molar balance

$$C_{gpi}G_i = C_{gps}G_{ds}. \tag{A-4}$$

At the near-ambient conditions used in this investigation, the Ideal Gas Law applied. Then $P_p = y_pP$ and

$$C_{gp} = P_p/RT = y_p P/RT. \tag{A-5}$$

For the gas flow upstream of the column inlet, this became, with standard pressure $P_s = 1$ atm,

$$C_{gps} = y_{ps} P_s/RT_s = y_{ps}/RT_s. \tag{A-6}$$

Substituting (A-6) into (A-4) gave

$$C_{gpi} G_i = (y_{ps}/RT_s) G_{ds} = y_{ps} G_{ds}/RT_s. \tag{A-7}$$

for which all quantitites on the right-hand side of the equality were known. Similarly, column outlet conditions were related to the final or sampling-point conditions by

$$C_{gpo} G_o = C_{gpf} G_f = (y_{pf} P_f/RT_f) G_f = y_{pf} G_f/RT_f, \tag{A-8}$$

for which all quantities were known except the sampling-point gas flow rate G_f.

For near-ambient temperature, pressure, and absolute humidity, wet gas flow rate is related to the equivalent dry gas and standard dry gas flow rates via

$$G = (G/G_d)(G_d/G_{ds}) G_{ds}. \tag{A-9}$$

For constant temperature and total pressure, absolute humidity varies proportionally with water vapor pressure P_v, and the ratio of wet to dry gas flow rates varies inversely with dry gas pressure $P_d = P - P_v$, or

$$G/G_d = P/P_d = P/(P - P_v). \tag{A-10}$$

For constant composition and varying temperature and pressure, dry and standard dry gas flow rates are related by

$$G_d/G_{ds} = (T/T_s)(P_s/P_d) = (T/T_s)P_s/(P - P_v). \tag{A-11}$$

Substituting (A-10) and (A-11) into (A-9) gave

$$G = G_{ds}(T/T_s)PP_s/(P - P_v)^2. \tag{A-12}$$

Applying this relationship to the sampling-point flow rate G_f gave, for $P_f = P_s = 1$ atm,

$$\begin{aligned} G_f &= G_{ds}(T_f/T_s)P_fP_s/(P_f - P_{vf})^2 \\ &= G_{ds}(T_f/T_s)/(1 - P_{vf})^2. \end{aligned} \tag{A-13}$$

Substituting (A-13) into (A-8) gave

$$\begin{aligned} C_{gpo}G_o &= y_{pf}[G_{ds}(T_f/T_s)/(1 - P_{vf})^2]/RT_f \\ &= y_{pf}G_{ds}/RT_s(1 - P_{vf})^2. \end{aligned} \tag{A-14}$$

Finally, substituting (A-14) and (A-7) into (A-3) gave

$$F_p = \{y_{ps} - [y_{pf}/(1 - P_{vf})^2]\} G_{ds}/RT_s V_c, \qquad \text{(A-15)}$$

for which all quantities on the right-hand side are known.

The percent removal of pollutant per unit height of a bubble column was defined as

$$\begin{aligned} R_h &= [(y_{pis} - y_{pos})/y_{pis}]\ 100/h_c \\ &= [1 - (y_{pos}/y_{pis})]\ 100/h_c, \end{aligned} \qquad \text{(A-16)}$$

where the input and output concentrations of pollutant are expressed as mole fractions of their respective gas phases at standard conditions (dry gas with T = 298 K and P = 1 atm). The inlet concentration y_{pis} is equal to the known standard upstream concentration y_{ps}, or

$$y_{pis} = y_{ps}. \qquad \text{(A-17)}$$

To relate the column outlet concentration y_{pos} to the sampled pollutant concentration y_{pf} required knowledge of the value of their ratio y_{pos}/y_{pf}. To this end, (A-5) and (A-8) were combined to give

$$G_f/G_o = C_{gpo}/C_{gpf} = (y_{po}/y_{pf})(T_f/T_o)(P_o/P_f). \qquad \text{(A-18)}$$

Solving for y_{po}/y_{pf} gave, with $P_o = P_f = 1$ atm,

$$y_{po}/y_{pf} = (T_o/T_f)(G_f/G_o). \qquad \text{(A-19)}$$

Now from (A-12),

$$G_o = G_{ds}(T_o/T_s)/(1 - P_{vo})^2, \tag{A-20}$$

and the ratio of (A-13) and (A-20) was

$$G_f/G_o = (T_f/T_o)(1 = p_{vo})^2/(1 - P_{vf})^2. \tag{A-21}$$

Then (A-21) into (A-19) gave

$$y_{po}/y_{pf} = (1 - P_{vo})^2/(1 - P_{vf})^2. \tag{A-22}$$

Similarly, with $P_{vs} = 0$,

$$y_{pos}/y_{po} = (1 - P_{vs})^2/(1 - P_{vo})^2 = 1/(1 - P_{vo})^2. \tag{A-23}$$

Combining (A-23) and A-22) gave

$$y_{pos}/y_{pf} = (y_{pos}/y_{po})(y_{po}/y_{pf}) = 1/(1 - P_{vf})^2 \tag{A-24}$$

and thus

$$y_{pos} = y_{pf}/(1 - P_{vf})^2. \tag{A-25}$$

Finally, (A-25) and (A-17) into (A-16) gave

$$R_h = \{1 - [y_{pf}/y_{ps}(1 - P_{vf})^2]\}\ 100/h_c, \tag{A-26}$$

for which all quantities on the right are known.

After the initial solubilization transient has passed (see Appendix B), the outlet pollutant concentration from a short bubble column must equal the inlet concentration. Expressing (A-23) in terms of inlet conditions and rearranging (with $y_{pis} = y_{ps}$ and $P_{vi} = P_{vo}$) gave

$$y_{pi} = y_{pis}(1 - P_{vi})^2 = y_{ps}(1 - P_{vo})^2. \qquad \text{(A-27)}$$

Solving (A-22) for y_{po} gave

$$y_{po} = y_{pf}(1 - P_{vo})^2/(1 - P_{vf})^2. \qquad \text{(A-28)}$$

Equating (A-27) and (A-28) and solving for y_{pf} gave

$$y_{pf} = y_{ps}(1 - P_{vf})^2. \qquad \text{(A-29)}$$

For the purpose of detector tube calculation, (A-29) allowed the actual sampled pollutant concentration to be calculated from the known source concentration.

APPENDIX B
DERIVATION OF SOLUBILIZATION TIME CONSTANT

When polluted gas is initially bubbled through a fresh charge of solution in an absorption column, the outlet concentration of pollutant (and other soluble gases) rises from zero to the steady-state value dictated by the total complex of absorbing conditions. A good first approximation for this time required to reach steady-state can be found by considering absorption into a single equilibrium stage with pure water as the absorbant.

Equilibrium of the gas and liquid at the outlet implies that the pollutant partial pressure P_{po} in the gas at the column outlet is related to the pollutant concentration C_{1p} in the homogeneous liquid via Henry's Law. With near-ambient conditions prevailing in the gas phase, $P_{po} = y_p P_o$, $P_o = P_s = 1$ atm, and

$$C_{1p} = P_{po}/H_p = y_{po}P_o/H_p = y_{po}/H_p. \qquad \text{(B-1)}$$

Since the difference between the molar flowrates of pollutant in the gas at the inlet and outlet must equal the total rate change in the water, molar balance for the column stage gave

$$V_1(dC_{1p}/dt) = C_{gpi}G_i - C_{gpo}G_o. \qquad \text{(B-2)}$$

Since a column of water 1048 cm high at $T_c = 50$ C will exert a gauge pressure of 1 atm at its base, a very short column ($h_c << 1048$ cm) will exert negligible pressure at its base compared with the 1048 cm column. Then $P_i \cong P_o = P_s = 1$ atm, and since $T_i = T_o = T_c$, ideal-gas conditions implied that

$$C_{gpi} = y_{pi}P_i/RT_i = y_{pi}/RT_c, \tag{B-3}$$

$$C_{gpo} = y_{po}P_o/RT_o = y_{po}/RT_c, \tag{B-4}$$

and

$$V_1(dC_{1p}/dt) = (y_{pi}G_i - y_{po}G_o)/RT_c. \tag{B-5}$$

$P_i = P_o$ and $T_i = T_o$ meant that $G_i = G_o = G_c$. Then

$$dC_{1p}/dt = (y_{pi} - y_{po})G_c/V_1RT_c. \tag{B-6}$$

Since H_p in (B-1) is usually constant with respect to concentration and time, dC_{1p}/dt became

$$dC_{1p}/dt = d(y_{po}/H_p)/dt = (dy_{po}/dt)/H_p. \tag{B-7}$$

Equating (B-7) and (B-6) and solving for dy_{po}/dt gave

$$dy_{po}/dt = (y_{pi} - y_{po})(G_cH_p/V_1RT_c). \tag{B-8}$$

Solving this differential equation for y_{po} with the boundary conditions $y_{po} = 0$ at $t = 0$ and $y_{po} = y_{pi}$ at $t = \infty$ gave

$$y_{po} = y_{pi}[1 - \exp(-t/t_c)], \tag{B-9}$$

where the time constant for this step-response function is

$$t_c = V_1 R T_c / G_c H_p. \tag{B-10}$$

Therefore, the time for the absorption column to reach its steady-state condition is not dependent on the pollutant inlet concentration y_{pi}.

Maximum t_c occurs at minimum gas flowrate G_c in the column. Since from (A-12)

$$G_c = G_{ds}(T_c/T_s)/(1 - P_{vc})^2, \tag{B-11}$$

the maximum t_c occurs at minimum P_{vc} for constant T_c and G_{ds}. Assuming $P_{vc} = 0$ as an extremum,

$$G_c = G_{ds}(T_c/T_s), \tag{B-12}$$

and (B-12) into (B-10) gave

$$(t_c)_{max} = V_1 R T_s / G_{ds} H_p. \tag{B-13}$$

After $t = 5t_c$,

$$y_{po} = 0.993\ y_{pi} \cong y_{pi}, \tag{B-14}$$

and steady-state conditions have effectively been reached.

BIOGRAPHICAL SKETCH

Gary Patrick Noyes was born and raised in Ft. Pierce, Florida. In 1968, he was awareded a B.S. with Honors in aerospace engineering by the University of Florida. After service in the U.S. Air Force as an aircraft engineering officer, Mr. Noyes held positions in environmental planning, telecommunications systems assembly supervision, and microelectronics engineering management. He received an M.E. in environmental engineering sciences from the University of Florida in 1977. Mr. Noyes is married and has two children. Upon graduation, he will be employed in the development of advanced life-support systems for spacecraft.

I certify that I have read this study and that in my opinion it conforms to acceptable standards of scholarly presentation and is fully adequate, in scope and quality, as a dissertation for the degree of Doctor of Philosophy.

John Zoltek, Jr., Chairman
Professor of Environmental Engineering
Sciences

I certify that I have read this study and that in my opinion it conforms to acceptable standards of scholarly presentation and is fully adequate, in scope and quality, as a dissertation for the degree of Doctor of Philosophy.

William B. Arbuckle
Assistant Professor of Environmental
Engineering Sciences

I certify that I have read this study and that in my opinion it conforms to acceptable standards of scholarly presentation and is fully adequate, in scope and quality, as a dissertation for the degree of Doctor of Philosophy.

James P. Heaney
Professor of Environmental Engineering
Sciences

I certify that I have read this study and that in my opinion it conforms to acceptable standards of scholarly presentation and is fully adequate, in scope and quality, as a dissertation for the degree of Doctor of Philosophy.

S. J. Locascio
Salvadore J. Locascio
Professor of Horticulture Sciences

I certify that I have read this study and that in my opinion it conforms to acceptable standards of scholarly presentation and is fully adequate, in scope and quality, as a dissertation for the degree of Doctor of Philosophy.

Paul Urone
Paul Urone
Professor of Environmental Engineering Sciences

This dissertation was submitted to the Graduate Faculty of the College of Engineering and to the Graduate Council, and was accepted as partial fulfillment of the requirements for the degree of Doctor of Philosophy.

August 1982

Hubert A. Bevis
Dean, College of Engineering

Dean, Graduate School

UNIVERSITY OF FLORIDA
3 1262 08666 917 2